
SAFE AND QUASI-OPTIMAL AUTONOMOUS NAVIGATION IN ENVIRONMENTS WITH CONVEX OBSTACLES

A PREPRINT

Ishak Cheniouni

Department of Electrical Engineering
Lakehead University
Thunder Bay, ON P7B 5E1, Canada
cheniouni@lakeheadu.ca

Soulaimane Berkane

Department of Computer Science and Engineering
University of Quebec in Outaouais
101 St-Jean Bosco, Gatineau, QC, J8X 3X7, Canada
soulaimane.berkane@uqo.ca

Abdelhamid Tayebi

Department of Electrical Engineering
Lakehead University
Thunder Bay, ON P7B 5E1, Canada
atayebi@lakeheadu.ca

ABSTRACT

We propose a continuous feedback control strategy that steers a point-mass vehicle safely to a destination, in a quasi-optimal manner, in sphere worlds. The main idea consists in avoiding each obstacle via the shortest path within the cone enclosing the obstacle and moving straight toward the target when the vehicle has a clear line of sight to the target location. In particular, almost global asymptotic stability of the target location is achieved in two-dimensional (2D) environments under a particular assumption on the obstacles configuration. We also propose a reactive (sensor-based) approach, suitable for real-time implementations in *a priori* unknown 2D environments with sufficiently curved convex obstacles, guaranteeing almost global asymptotic stability of the target location. Simulation results are presented to illustrate the effectiveness of the proposed approach.

Keywords Autonomous navigation · Obstacle avoidance · Feedback control

1 Introduction

1.1 Motivation

Autonomous navigation consists in steering a robot from an initial position to a final destination while avoiding obstacles. The existing solutions for this problem can be classified into two main approaches. The first approach is the plan-and-track approach, which consists in generating, from a map of the environment, a collision-free path to be tracked via a feedback controller. The second approach, referred to as feedback-based approach, is a direct approach which consists in designing, **in one shot**, a feedback control strategy that steers the robot to the target location along a collision-free path. While safe global (or almost global) convergence to a target is achieved in environments with specific geometries, the existing feedback-based approaches do not generally generate the shortest collision-free paths. In this paper, we address this problem by proposing a continuous quasi-optimal¹ feedback control strategy guaranteeing safe and quasi-optimal navigation in n -dimensional sphere worlds and two-dimensional arbitrary convex environments.

A preliminary version of the present work has been presented in the 2023 American Control Conference Cheniouni et al. [2023]. Soulaimane Berkane is also with the Department of Electrical Engineering, Lakehead University, Thunder Bay, ON P7B 5E1, Canada.

¹This term will be rigorously defined later.

1.2 Prior Literature

Among the path-finding algorithms of the plan-and-track category, one can cite the Dijkstra algorithm [Dijkstra, 1959] or the A* (A star) algorithm [Hart et al., 1968], which rely on grids or graphs representing the environment where the shortest path is determined. One can also find reactive motion planning algorithms, such as the family of Bug algorithms [Lumelsky and Stepanov, 1986, Lumelsky and Skewis, 1990] which are used to navigate in planar environments without guarantees on the optimality of the generated paths. Artificial potential field methods are an example of a feedback-based approach. They consider a robot moving in a force field where the destination generates an attractive force, and the obstacles generate repulsive forces [Khatib, 1986]. The destination is the minimum of the potential function, and the negative gradient leads safely to it. These methods suffer from two problems, namely, the generation of local minima where the robot may get trapped instead of reaching the goal, and if the goal is reached the generated path is not generally the shortest collision-free path. To address local minima problem, the authors in [Koditschek and Rimon, 1990] proposed a navigation function (NF) whose negative gradient is the control law that steers the robot from almost all initial conditions to the target location in an *a priori* known sphere world. In order to navigate in more general spaces, diffeomorphisms from sphere worlds to more complex worlds were proposed in [Rimon and Koditschek, 1991, 1992]. The authors in [Loizou, 2011, Constantinou and Loizou, 2020] proposed tuning-free navigation functions and diffeomorphisms from a point world to a sphere world or a star world. A sufficient condition was given in [Paternain et al., 2018] for an artificial potential to be a navigation function in environments containing smooth, non-intersecting, and strongly convex obstacles. More recently, a tuning-free navigation function based on harmonic functions has been proposed in [Loizou and Rimon, 2021] for sensor-based autonomous navigation [Loizou, 2011, Constantinou and Loizou, 2020].

In [Arslan and Koditschek, 2019], the authors proposed a new sensor-based autonomous navigation strategy (different from the NF-based approach) by constructing a compact obstacle-free local set around the robot using the hyperplanes separating the robot from the neighboring obstacles and then steering the robot towards the projection of the target location onto the boundary of this compact set. This approach ensures safe navigation through unknown strongly convex obstacles and convergence to the destination from everywhere, except from a set of zero Lebesgue measure. This work has been extended for non-convex star-shaped obstacles in [Vasilopoulos and Koditschek, 2018], and polygonal obstacles with possible overlap in [Vasilopoulos et al., 2020]. A sensor-based autonomous navigation approach, relying on Nagumo's theorem [Nagumo, 1942] and using tangent cones, was proposed in [Berkane, 2021]. This approach guarantees safety through an appropriate switching between a stabilizing controller and an obstacle avoidance controller. Control Barrier Functions (CBFs) and Control Lyapunov Functions (CLFs) were used in [Ames et al., 2014, 2017] along with a quadratic program to design navigation controllers ensuring the stabilization of the desired target location with safety guarantees. Hybrid feedback was used, for instance in [Sanfelice et al., 2006, Berkane et al., 2022, Sawant et al., 2023a], to achieve global convergence; a feature that is not possible to obtain via continuous time-invariant control due to topological obstructions [Koditschek and Rimon, 1990].

1.3 Contributions

The present paper proposes a continuous quasi-optimal feedback control strategy for safe autonomous navigation in n -dimensional sphere words and two-dimensional environments with arbitrary convex and sufficiently curved obstacles. Our approach relies on iteratively projecting the nominal feedback controller on the obstacles' enclosing cones for known environments, which generates locally optimal collision-free trajectories. A sensor-based implementation of our control approach is proposed for *a priori* unknown 2D environments with arbitrary convex and sufficiently curved obstacles. The main contributions of the proposed approach are summarized as follows:

- The proposed feedback control law is continuous and ensures local optimal avoidance maneuvers with a high likelihood of generating an overall optimal path as illustrated via extensive simulations.
- Except for the restrictions imposed by the standard separation conditions of Assumptions 1, 2, the environment can be highly dense, and the destination can be located arbitrarily close to the obstacle boundaries.
- The reactive (sensor-based) version of our approach applies to *a priori* unknown 2D environments with arbitrary convex and sufficiently curved obstacles, and ensures almost global asymptotic stabilization of the target location.

1.4 Organization

The remainder of this paper is organized as follows: Section II provides the preliminaries that will be used throughout this article. In Section III, we formulate our autonomous navigation problem. In Section IV, we define the subsets of the free space that are needed for our proposed control design and we classify the obstacles, according to their visibility

from the destination, into different generations. In Sections V–VII, we present our control strategy and its properties. In Section VIII, our control strategy is adapted to the sensor-based scenarios in two-dimensional sphere worlds and sufficiently curved convex worlds. Simulation results are presented in Section X.

2 Notations and Preliminaries

Throughout the paper, \mathbb{N} , \mathbb{R} and $\mathbb{R}_{>0}$ denote the set of natural numbers, real numbers and positive real numbers, respectively. The Euclidean space and the unit n -sphere are denoted by \mathbb{R}^n and \mathbb{S}^n , respectively. The Euclidean norm of $x \in \mathbb{R}^n$ is defined as $\|x\| := \sqrt{x^\top x}$ and the angle between two non-zero vectors $x, y \in \mathbb{R}^n$ is given by $\angle(x, y) := \cos^{-1}(x^\top y / \|x\|\|y\|)$. The Jacobian matrix of a vector field $f : \mathbb{R}^n \rightarrow \mathbb{R}^n$ is given by $J_x(f(x)) = [\nabla_x f_1 \dots \nabla_x f_n]^\top$ where $\nabla_x f_i = [\frac{\partial f_i}{\partial x_1} \dots \frac{\partial f_i}{\partial x_n}]^\top$ is the gradient of the i -th element f_i . Define the ball centered at $x \in \mathbb{R}^n$, of radius $r \in \mathbb{R}_{>0}$, by the set $\mathcal{B}(x, r) := \{q \in \mathbb{R}^n \mid \|q - x\| \leq r\}$. The interior and the boundary of a set $\mathcal{A} \subset \mathbb{R}^n$ are denoted by $\mathring{\mathcal{A}}$ and $\partial\mathcal{A}$, respectively. The relative complement of a set $\mathcal{B} \subset \mathbb{R}^n$ with respect to a set \mathcal{A} is denoted by $\mathcal{B}_{\mathcal{A}}^c$. The distance of a point $x \in \mathbb{R}^n$ to a closed set \mathcal{A} is defined as $d(x, \mathcal{A}) := \min_{q \in \mathcal{A}} \|q - x\|$. The Minkowski sum of two convex sets \mathcal{A} and \mathcal{B} is defined as $\mathcal{A} \oplus \mathcal{B} := \{a + b \mid a \in \mathcal{A}, b \in \mathcal{B}\}$. The cardinality of a set $\mathcal{N} \subset \mathbb{N}$ is denoted by $\text{card}(\mathcal{N})$. The line segment connecting two points $x, y \in \mathbb{R}^n$ is defined as $\mathcal{L}(x, y) := \{q \in \mathbb{R}^n \mid q = x + \delta(y - x), \delta \in [0, 1]\}$. The parallel and orthogonal projections are defined as follows:

$$\pi^{\parallel}(a) := aa^\top, \quad \pi^{\perp}(a) := I_n - aa^\top, \quad (1)$$

where $I_n \in \mathbb{R}^{n \times n}$ is the identity matrix and $a \in \mathbb{S}^{n-1} \setminus \{0\}$. Therefore, for any vector x , the vectors $\pi^{\parallel}(a)x$ and $\pi^{\perp}(a)x$ correspond, respectively, to the projection of x onto the line generated by a and onto the hyperplane orthogonal to a . A hyperplane passing through $x \in \mathbb{R}^n$ and orthogonal to $v \in \mathbb{R}^n \setminus \{0\}$ is defined as $\mathcal{P}_\Delta(x, v) := \{q \in \mathbb{R}^n \mid v^\top(q - x) \Delta 0\}$ where $\Delta \in \{=, \leq, <, \geq, >\}$. When $\Delta \in \{\leq, <, \geq, >\}$, the hyperplane divides the space into two half-spaces where “ \leq ” (resp. “ $<$ ”) represents the closed negative half-space (resp. the open negative half-space), and “ \geq ” (resp. “ $>$ ”) represents the closed positive half-space (resp. the open positive half-space). A conic subset of $\mathcal{A} \subseteq \mathbb{R}^n$, with vertex $x \in \mathbb{R}^n$, axis $a \in \mathbb{R}^n$, and aperture 2ψ is defined as follows [Berkane et al., 2019]:

$$\mathcal{C}_{\mathcal{A}}^\Delta(x, a, \psi) := \{q \in \mathcal{A} \mid \|a\|\|q - x\| \cos(\psi) \Delta a^\top(q - x)\}, \quad (2)$$

where $\psi \in (0, \frac{\pi}{2}]$ and $\Delta \in \{\leq, <, =, >, \geq\}$, with “ $=$ ”, representing the surface of the cone, “ \leq ” (resp. “ $<$ ”) representing the interior of the cone including its boundary (resp. excluding its boundary), and “ \geq ” (resp. “ $>$ ”) representing the exterior of the cone including its boundary (resp. excluding its boundary). The set of vectors parallel to the cone $\mathcal{C}_{\mathbb{R}^n}^\pm(x, a, \psi)$ is defined as follows:

$$\mathcal{V}(a, \psi) := \{v \in \mathbb{R}^n \mid v^\top a = \|v\|\|a\| \cos(\psi)\}. \quad (3)$$

3 Problem Formulation

Consider a point mass vehicle at position $x \in \mathbb{R}^n$ moving inside a spherical workspace $\mathcal{W} \subset \mathbb{R}^n$ centered at the origin 0 and punctured by $m \in \mathbb{N}$ balls \mathcal{O}_i such that:

$$\mathcal{W} := \mathcal{B}(0, r_0), \quad (4)$$

$$\mathcal{O}_i := \mathcal{B}(c_i, r_i), \quad i \in \mathbb{I} := \{1, \dots, m\}, \quad (5)$$

where $r_0 > r_i > 0$ for all $i \in \mathbb{I}$. The free space is, therefore, given by the closed set

$$\mathcal{F} := \mathcal{W} \setminus \bigcup_{i=1}^m \mathcal{O}_i. \quad (6)$$

For \mathcal{F} to be a valid sphere world, as defined in [Koditchev and Rimon, 1990], the obstacles \mathcal{O}_i must satisfy the following assumptions:

Assumption 1. *The obstacles are completely contained within the workspace and separated from its boundary, i.e.,*

$$\min_{a \in \mathcal{O}_i, b \in \partial\mathcal{W}} \|a - b\| > 0, \quad \forall i \in \mathbb{I}. \quad (7)$$

Assumption 2. *The obstacles are disjoint, i.e.,*

$$\min_{a \in \mathcal{O}_i, b \in \mathcal{O}_j} \|a - b\| > 0, \quad \forall i, j \in \mathbb{I}, i \neq j. \quad (8)$$

Consequently, the boundary of the free space \mathcal{F} is given by

$$\partial\mathcal{F} := \partial\mathcal{W} \bigcup \left(\bigcup_{i=1}^m \partial\mathcal{O}_i \right). \quad (9)$$

Consider the following first-order dynamics

$$\dot{x} = u, \quad (10)$$

where u is the control input. The objective is to determine a continuous Lipschitz state-feedback controller $u(x)$ that safely steers the vehicle from almost any initial position $x(0) \in \mathcal{F}$ to any given desired destination $x_d \in \bar{\mathcal{F}}$. In particular, the closed-loop system

$$\dot{x} = u(x), \quad x(0) \in \mathcal{F} \quad (11)$$

must ensure forward invariance of the set \mathcal{F} , almost global asymptotic stability of the equilibrium $x = x_d$, and *quasi-optimal obstacle avoidance maneuver*. A quasi-optimal obstacle avoidance maneuver is defined as follows. Let $x(t)$ be the generated trajectory of the closed-loop system (11), such that $\lim_{t \rightarrow \infty} x(t) = x_d$. For some $\varepsilon \geq 0$ and for each $i \in \mathcal{VO} \subseteq \mathbb{I}$, where \mathcal{VO} is the ordered list of visited obstacles, let $x_{d,\varepsilon}^i$ denote the point where the curve $x(t)$ leaves the ball $\mathcal{B}(c_i, r_i + \varepsilon)$ enclosing the i th obstacle, with $x_{d,\varepsilon}^z := x_d$ and $z = \text{card}(\mathcal{VO})$. Also, let $x_{0,\varepsilon}^i := x_d^{i-1}$ with $x_{0,\varepsilon}^1 := x(0)$.

Definition 1. The trajectory $x(t)$ is said to be generated by a quasi-optimal obstacle avoidance maneuver if there exists $\varepsilon \geq 0$ such that the local obstacle avoidance maneuvers, with respect to each obstacle i and between $x_{0,\varepsilon}^i$ and $x_{d,\varepsilon}^i$, are all optimal (i.e., they generate the shortest collision-free Euclidean paths).

4 Sets Definition and Obstacles Classification

In this section, we define the subsets of the free space that are needed for our proposed control design in Section 5. These are given as follows:

- The hat of a cone inside the workspace \mathcal{W} , enclosing an obstacle \mathcal{O}_i , of vertex $y \in \mathbb{R}^n$ and aperture θ_i is defined as follows (orange region in Fig. 1):

$$\mathcal{H}(y, c_i) := \{q \in \mathcal{C}_{\mathcal{W}}^{\leq}(y, c_i - y, \theta_i(y)) | (c_i - q)^T (y - q) \leq 0\}, \quad (12)$$

where the angle $\theta_i(y) = \arcsin(r_i/\|c_i - y\|) \in (0, \frac{\pi}{2}]$.

- The shadow region: the area where the vehicle does not have a clear line of sight to the target is defined as follows (blue region in Fig. 1):

$$\mathcal{D}(x_d, c_i) := \{q \in \mathcal{C}_{\mathcal{F}}^{\leq}(x_d, c_i - x_d, \phi_i) | (c_i - q)^T (x_d - q) \geq 0\}, \quad (13)$$

where the angle $\phi_i = \arcsin(r_i/\|c_i - x_d\|) \in (0, \frac{\pi}{2}]$.

- The exit set separates the set $\mathcal{D}(x_d, c_i)$ and its complement with respect to \mathcal{F} and is defined as follows (thick blue lines in Fig. 1):

$$\mathcal{S}(x_d, c_i) := \{q \in \mathcal{C}_{\mathcal{F}}^=(x_d, c_i - x_d, \phi_i) | (c_i - q)^T (x_d - q) \geq 0\}. \quad (14)$$

Next, we classify the obstacles according to their visibility from the destination into different generations. An obstacle that can be fully seen from the destination is a *first-generation obstacle* (dark gray obstacles $\{1, 2, 3\}$ in Fig. 2). A *second-generation obstacle* can be partially seen from the destination and is partially included in the shadow regions of the first-generation obstacles (medium gray obstacles $\{4, 5\}$ in Fig. 2). An obstacle is said to be of generation ($j \geq 2$) if it is partially seen from the destination and partially included in the shadow region of at least one obstacle of generation ($j - 1$), which must be the highest generation among the generations of obstacles shadowing the considered obstacle (e.g., obstacle 6, in Fig. 2, is of generation 3 since it is partially shadowed by obstacle 4 (of generation 2) even if it is also partially shadowed by obstacle 1 (of generation 1)). An obstacle that is completely hidden from the destination, whose shadow region is entirely included in the shadow regions of other obstacles, is classified as a *zero-generation obstacle* (white obstacles in Fig. 2). Now, we define the sets related to the obstacle classification as follows (see Fig. 2):

- The sub-shadow region of an obstacle \mathcal{O}_i of generation j is defined as follows:

$$\mathcal{D}^j(x_d, c_i) := \mathcal{D}(x_d, c_i) \setminus \bigcup_{l=1}^{j-1} \left[\bigcup_{k \in J_i^l} \mathcal{D}^l(x_d, c_k) \right], \quad (15)$$

for $j \geq 2$ where $J_i^j = \{k \in \{1, \dots, m\} | k \neq i \text{ and } \mathcal{D}(x_d, c_i) \cap \mathcal{D}^j(x_d, c_k) \neq \emptyset\}$ is the set of the j -generation obstacles that include obstacle i in their sub-shadow regions and $\mathcal{D}^1(x_d, c_i) = \mathcal{D}^0(x_d, c_i) := \mathcal{D}(x_d, c_i)$.

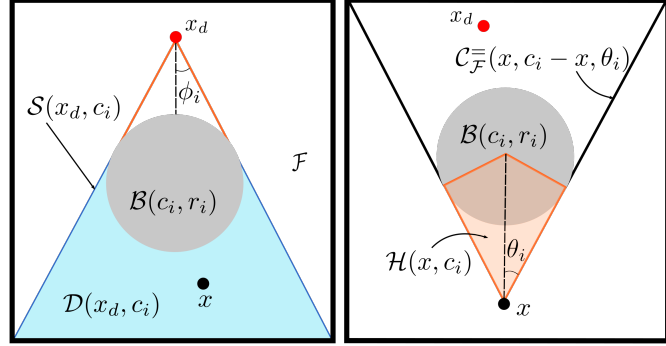


Figure 1: 2D representation of the sets in Section 4.

- The blind set is a subset of \mathcal{F} where there is no line of sight to the destination, and it is defined as

$$\mathcal{BL} := \bigcup_{j=1}^s \left[\bigcup_{i \in \mathcal{G}_j} \mathcal{D}^j(x_d, c_i) \right], \quad (16)$$

where \mathcal{G}_j is the set of obstacles of generation $j \in \{1, \dots, s\}$ and $s \leq m$ is the total number of generations in the workspace.

- The visible set is defined as the complement of the blind set with respect to the free space $\mathcal{VI} := \mathcal{BL}_{\mathcal{F}}^c$.

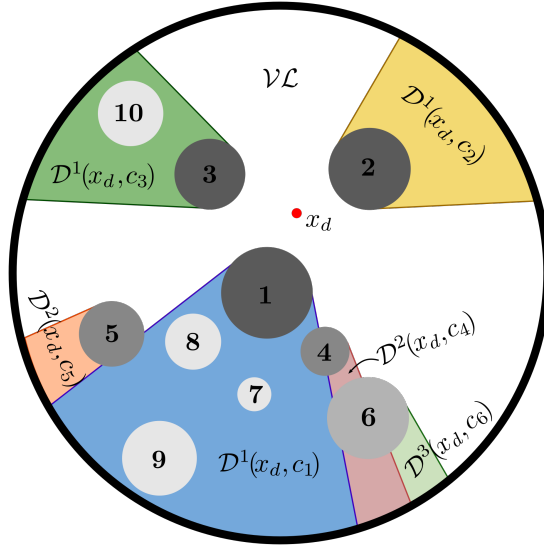


Figure 2: Illustration of the sub-shadow regions of obstacles from different classes in a two-dimensional sphere world. First-generation obstacles are in dark gray, second-generation obstacles are in medium gray, third-generation obstacles are in light gray and zero-generation obstacles are in white.

5 Control Design

5.1 Single Obstacle Case

Let us start by considering a single obstacle \mathcal{O}_i and ignoring all others. We design a preliminary control law for the single obstacle case, which will be used as a baseline in the multiple obstacle case. First, in the case where the path is clear (*i.e.*, x belongs to the visible set \mathcal{VI}), the vehicle follows a straight line to the destination under the control law $u_d(x) = -\gamma(x - x_d)$ where $\gamma \in \mathbb{R}_{>0}$. Next, in the case where the path is not clear (*i.e.*, $x \in \mathcal{D}(x_d, c_i)$), we generate a control input (vehicle's velocity) that is in the direction of the cone $\mathcal{C}_{\mathcal{F}}^-(x, c_i - x, \theta_i)$ enclosing the obstacle while

ensuring that the control input is equal to $u_d(x)$ at the exit set $\mathcal{S}(x_d, c_i)$, defined in (14). In particular, the direction of the control input should minimize the angle between the nominal control direction, given by $(x_d - x)$, and the set of all vectors parallel to the enclosing cone, *i.e.*, the control input should belong to the set

$$\mathcal{U}_1(x) := \arg \min_{v_i \in \mathcal{V}(c_i - x, \theta_i)} \angle(x_d - x, v_i). \quad (17)$$

Moreover, to ensure continuity of the control input, we impose further that the control input belongs to the set

$$\mathcal{U}_2(x) := \{v \in \mathbb{R}^n : v = u_d(x) \text{ when } x \in \mathcal{S}(x_d, c_i)\}. \quad (18)$$

These two conditions can be written as follows

$$u(x) \in \mathcal{U}_1(x) \cap \mathcal{U}_2(x). \quad (19)$$

In the following lemma, it is shown that the set $\mathcal{U}_1(x) \cap \mathcal{U}_2(x)$ is a singleton and the unique solution is provided.

Lemma 1. *Set $\mathcal{U}_1(x) \cap \mathcal{U}_2(x)$ is a singleton and its unique element is given by*

$$u(x) = \xi(u_d(x), x, i), \quad (20)$$

where $\xi : \mathbb{R}^n \times \mathbb{R}^n \times \mathbb{N} \rightarrow \mathbb{R}^n$ is given by

$$\xi(u, x, i) := \frac{\sin(\beta_i(u, x)) \sin^{-1}(\theta_i(x))}{\cos(\theta_i(x) - \beta_i(u, x))} \pi^{\parallel}(\bar{\xi}_i) u, \quad (21)$$

with $\bar{\xi}_i \in \mathcal{V}(c_i - x, \theta_i)$,

$$\bar{\xi}_i := \frac{\sin(\theta_i(x)) u}{\sin(\beta_i(u, x)) \|u\|} - \frac{\sin(\theta_i(x) - \beta_i(u, x))}{\sin(\beta_i(u, x))} \frac{(c_i - x)}{\|c_i - x\|}, \quad \beta_i(u, x) := \angle(u, c_i - x) \leq \theta_i(x).$$

Proof. See Appendix 9. \square

In other words, Lemma 1 shows that, when $x \in \mathcal{D}(x_d, c_i)$, the control $u(x)$ is a scaled parallel projection of the nominal controller $u_d(x)$ in the direction of $\bar{\xi}_i$ which represents a unit vector on the cone enclosing the obstacle. Finally, one obtains the following control strategy in the case of a single obstacle

$$u(x) = \begin{cases} u_d(x), & x \in \mathcal{VI}, \\ \xi(u_d(x), x, i), & x \in \mathcal{D}(x_d, c_i). \end{cases} \quad (22)$$

Note that, during the avoidance maneuver, the controller depends on three arguments: the nominal control $u_d(x)$, the current position of the vehicle x , and the obstacle index i . Moreover, the trajectory of the closed-loop system (10)-(22) generates an optimal obstacle avoidance maneuver as shown in the following lemma.

Lemma 2. *The path generated by the closed-loop system (10)-(22) is the shortest path to the destination x_d from every initial condition $x(0) \in \mathcal{F} \setminus \mathcal{L}_d(x_d, c_i)$ where $\mathcal{L}_d(x_d, c_i) := \{q \in \mathcal{D}(x_d, c_i) \mid q = c_i + \delta(c_i - x_d), \delta \in \mathbb{R}_{>0}\}$.*

Proof. See Appendix 9. \square

5.2 Multiple Obstacles Case

In the case of multiple obstacles and when $x \in \mathcal{BL}$, one proceeds with multiple projections as described hereafter. When $x \in \mathcal{BL}$, there exist a unique $j \in \{1, \dots, s\}$ and a unique $i \in \mathcal{G}_j$ such that $x \in \mathcal{D}^j(x_d, c_i)$ (see equation (16)). In this case, the obstacle \mathcal{O}_i is the first to be considered, and $u_d(x)$ is projected onto its enclosing cone in a similar way as in (22). The resulting control vector is denoted by $u_1(x)$. The next obstacle to be considered is selected from the set of obstacles intersecting the hat of the cone enclosing obstacle \mathcal{O}_i defined as $\mathcal{LO}_i(x) := \{k \in \mathbb{I} \setminus \{i\} \mid \mathcal{O}_k \cap \mathcal{H}(x, c_i) \neq \emptyset\}$, see Fig. 3. Amongst obstacles in $\mathcal{LO}_i(x)$ that contain u_1 in their enclosing cones (*i.e.*, $k \in \mathcal{LO}_i(x)$, $u_1 \in \mathcal{V}(c_k - x, \theta_k)$), one chooses the closest in terms of the Euclidean distance to \mathcal{O}_i . If $\mathcal{LO}_i(x) = \emptyset$ or no obstacle contains u_1 in its enclosing cone, the path is free. Otherwise, u_1 will be considered as u_d for the new selected obstacle and the same approach is followed to obtain u_2 . Obstacle \mathcal{O}_i is called an ancestor to the selected obstacle and the selection and projection is repeated until the path is free (see Fig. 3). The obstacles selected during the successive projections at a position x , are grouped in an ordered list $\mathcal{I}(x) \subset \mathbb{I}$ from the first obstacle (\mathcal{O}_i , such that $x \in \mathcal{D}^j(x_d, c_i)$) to the last one (obstacle involved in the last projection). Let $h(x) = \text{card}(\mathcal{I}(x))$ be the number of required projections at position x . Define the map $\iota_x : \{1, \dots, h(x)\} \rightarrow \mathcal{I}(x)$ which associates to each projection $p \in \{1, \dots, h(x)\}$ the corresponding obstacle $\iota_x(p) \in \mathcal{I}(x)$. The set of positions involving obstacle k in the successive projections is called active region and

defined as $\mathcal{AR}_k := \{q \in \mathcal{BL} \mid k \in \mathcal{I}(q)\}$. To sum up, the intermediary control at a step $p \in \{1, \dots, h(x)\}$ and position $x \in \mathcal{AR}_{\iota_x(p)}$ is given by the recursive formula

$$u_p(x) = \xi(u_{p-1}(x), x, \iota_x(p)), \quad (23)$$

with $u_0(x) = u_d(x)$ and $\xi(\cdot, \cdot, \cdot)$ as defined in Lemma 1. Finally, the proposed control law is obtained by performing $h(x)$ successive projections and is given by

$$u(x) = \begin{cases} u_d(x), & x \in \mathcal{VI}, \\ u_{h(x)}(x), & x \in \mathcal{BL}. \end{cases} \quad (24)$$

The selection of the obstacles of the set $\mathcal{I}(x)$ is performed through the process summarized in Algorithm 1, and the

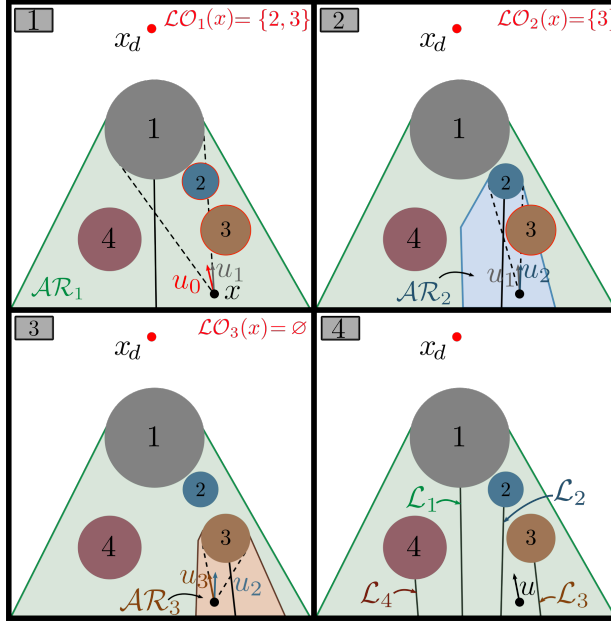


Figure 3: Successive projections of the control u_d in a two-dimensional sphere world with four obstacles.

implementation of the control strategy (24) is summarized in Algorithm 2.

Remark 1. It is worth pointing out that the successive projections, involved in the control design, start from the closest obstacle to the destination. This approach enables our controller to enjoy the following features: 1) generates shortest paths; 2) guarantees the continuity of the control input.

6 Safety and Stability Analysis

In this section, the safety and stability of the trajectories of the closed-loop system (10)-(24) will be analyzed. Nagumo's theorem ([Nagumo, 1942, Blanchini and Miani, 2007]), offers an important tool to prove safety. One of the statements of this theorem is the one based on Bouligand's tangent cones.

Definition 2. Given a closed set \mathcal{K} , the tangent cone to \mathcal{K} at x is $\mathcal{T}_{\mathcal{K}}(x) := \{z : \lim_{\tau \rightarrow 0} \inf \tau^{-1} d(x + \tau z, \mathcal{K}) = 0\}$.

In our case, when $x \in \mathcal{F}$, the tangent cone is the Euclidean space ($\mathcal{T}_{\mathcal{F}}(x) \equiv \mathbb{R}^n$), and since the free space is a sphere world (smooth boundary), the tangent cone at its boundary is a half-space (see Fig. 4). Nagumo's theorem guarantees, in a navigation problem, that the robot stays inside the free space \mathcal{F} . For Nagumo's condition to be satisfied, the velocity vector $u(x)$ must point inside (or is tangent to) the free space [Berkane, 2021]. In what follows, we rely on Nagumo's theorem to prove the safety of the trajectories generated by our closed-loop system.

Lemma 3 (Safety). Consider the closed set \mathcal{F} described in (6) and the kinematic system (10) under the control law (24). Then, the closed-loop system (10)-(24) admits a unique solution for all $t \geq 0$ and the set \mathcal{F} is forward invariant.

Proof. See Appendix 9. □

Algorithm 1 Obstacle selection for successive projections

Input: k index of the ancestor obstacle, v the resultant control from the projection onto the cone enclosing the ancestor obstacle, and the position $x(t)$.

Output: i index of the selected obstacle for the next projection.

```

1: if  $\mathcal{LO}_k = \emptyset$  then
2:    $i \leftarrow \{\emptyset\}$ ;
3: else
4:   Initialisation :  $L = \emptyset$ 
5:   for  $j \in \mathcal{LO}_k$  do
6:     if  $v \in \mathcal{V}(c_j - x, \theta_j)$  then
7:        $L = L \cup \{j\}$ ;
8:     end if
9:   end for
10:  if  $L = \emptyset$  then
11:     $i \leftarrow \{\emptyset\}$ ;
12:  else
13:     $i \leftarrow \arg \min_{j \in L} d(\mathcal{O}_k, \mathcal{O}_j)$ 
14:  end if
15: end if
16: return  $i$ 
```

Algorithm 2 Implementation of the control law (24) at an instant t

Input: $x(t)$.

Output: u .

```

Initialisation :  $u = u_d$ 
1: if  $x(t) \in \mathcal{BL}$  then
2:   Determine the obstacle  $i \in \mathbb{I}$  and its generation  $j \in \mathcal{G}$  such that  $x \in \mathcal{D}^j(x_d, c_i)$ .
3:   while  $i \neq \{\emptyset\}$  do
4:     Update  $u$  using (23) and considering obstacle  $i$ .
5:     Update  $i$  using Algorithm 1.
6:   end while
7: end if
8: return  $u$ 
```

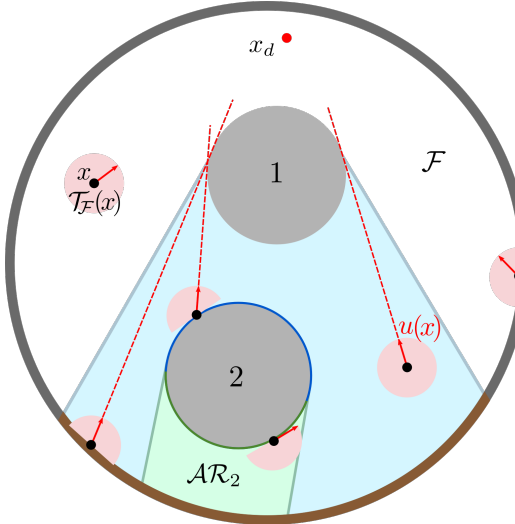


Figure 4: Bouligand's tangent cones.

Let us look for the equilibria of the closed-loop system (10)-(24) by setting $u(x) = 0$ in (24). Then, from the first equation of (24), the equilibrium point is x_d . From (23), one can rewrite the control at step $p \in \{1, \dots, h(x)\}$ and

position $x \in \mathcal{AR}_{\iota_x(p)}$, as $u_p = \sin(\beta_i) \sin^{-1}(\theta_i) \|u_{p-1}\| \xi_i^3$ where $\iota_x(p) = i$. In the case where $u_{p-1} \neq 0$, and since $\xi_i \in \mathbb{S}^{n-1}$, $u_p = 0$ if and only if $\beta_i = 0$. The set of positions leading to $\beta_i = 0$ is the segment (or segments) of the line, tangent to the ancestor obstacle $k = \iota_x(p-1)$, crossing the center of obstacle i , within the active region of obstacle i . When $\beta_i = 0$, the control input, at step $p-1$, is aligned with $(c_i - x)$, which is also tangent to the ancestor of obstacle i . We define the set of undesired equilibria (shown in Fig. 3) generated by obstacle i as follows:

$$\mathcal{L}_i := \{q \in \mathcal{AR}_i \mid \beta_i(u_{p-1}(q), q) = 0, p = \iota_q^{-1}(i)\}. \quad (25)$$

The central half-line generated by obstacle i in the workspace, starts from the center c_i and extends the set of undesired equilibria \mathcal{L}_i (as shown in Fig. 5), and is defined as follows:

$$\mathcal{L}_i^e := \left\{ q \in \mathcal{W} \mid q = c_i + \delta \frac{y - c_i}{\|y - c_i\|}, y \in \mathcal{L}_i, \delta \in \mathbb{R}_{>0} \right\}. \quad (26)$$

Some obstacles may not generate undesired equilibria, in specific configurations, as will be shown later, and in this case \mathcal{L}_i and \mathcal{L}_i^e are empty sets. Therefore, $u(x) = 0$ if $x \in \mathcal{L}_i$ where $i \in \mathcal{Z}$ and \mathcal{Z} is the set of obstacles generating undesired equilibria. Finally, one can conclude that the set of equilibrium points of the system (10)-(24) is given by $\zeta := \{x_d\} \cup (\cup_{i \in \mathcal{Z}} \mathcal{L}_i)$. The previous developments can be summarized in the following lemma:

Lemma 4. All trajectories of the closed-loop system (10)-(24) converge to the set $\zeta = \{x_d\} \cup (\cup_{i \in \mathcal{Z}} \mathcal{L}_i)$. \square

The indices of obstacles crossed by the central half-line \mathcal{L}_i^e of obstacle \mathcal{O}_i are grouped in the set defined as $\mathcal{M}_i := \{j \in \mathbb{I} \setminus \{i\} \mid \mathcal{L}_i^e \cap \mathcal{O}_j \neq \emptyset\}$ and $N_i = \text{card}(\mathcal{M}_i)$. Define the map $\kappa_i : \mathcal{M}_i \rightarrow \{1, \dots, N_i\}$ that associates to each index $k \in \mathcal{M}_i$ the corresponding order of the obstacle \mathcal{O}_k according to its proximity with respect to obstacle \mathcal{O}_i among the obstacles of indices in the set \mathcal{M}_i , where the order goes from the closest to the farthest obstacle. The set $\mathcal{M}_i^p := \{\kappa_i^{-1}(1), \dots, \kappa_i^{-1}(p)\}$, $p \leq N_i$, contains the indices of the set \mathcal{M}_i representing the p first obstacles in increasing order of their distance from obstacle i , and $\mathcal{M}_i^0 := \emptyset$. In the following lemma, we show that under certain conditions, obstacles in the set \mathcal{M}_i can be spared from generating undesired equilibria.

Lemma 5. Let $i \in \mathbb{I}$ such that $\mathcal{M}_i \neq \emptyset$. Obstacles of indices in the set \mathcal{M}_i^p , where $p \leq N_i$, do not generate undesired equilibria if, for all $k \in \mathcal{M}_i^p$, the following conditions are satisfied:

1. $c_k \in \mathring{\mathcal{H}}(x_{k,i}^*, c_i) \cup (\cup_{j \in \mathcal{M}_i^{p-1}} \mathring{\mathcal{H}}(x_{k,i}^*, c_j))$,
2. $(\mathring{\mathcal{H}}(x_{k,i}^*, c_i) \cup (\cup_{j \in \mathcal{M}_i^{p-1}} \mathring{\mathcal{H}}(x_{k,i}^*, c_j))) \cap \mathcal{O}_l = \emptyset$ for all $l \in \mathbb{I} \setminus (\mathcal{M}_i^p \cup \{i\})$,

where $x_{k,i}^* = \arg \max_{q \in \mathcal{L}_i^e \cap \partial \mathcal{O}_k} \|c_i - q\|$. Moreover, if $p = N_i$, or ($p < N_i$ and the obstacle of index $k = \kappa_i^{-1}(p+1)$ does not satisfy conditions 1) and 2)), the set \mathcal{M}_i is said to be of order $\bar{N}_i = p$ which is the total number of obstacles, of indices in the set \mathcal{M}_i , that do not generate undesired equilibria and the set $\mathcal{M}_i^{\bar{N}_i}$ groups them.

Proof. See Appendix 9. \square

Lemma 5 provides sufficient conditions for the first p obstacles, with indices in the set \mathcal{M}_i and ordered according to their proximity with respect to obstacle \mathcal{O}_i , to be free of undesired equilibria, and if $p = N_i$, or ($p < N_i$ and the $(p+1)$ -th obstacle does not satisfy these conditions), the set $\mathcal{M}_i^{\bar{N}_i}$ groups all the obstacles, with indices in the set \mathcal{M}_i , which do not generate undesired equilibria where $\bar{N}_i = p$ is the number of these obstacles and the order of the set \mathcal{M}_i . Fig. 5 shows an example of a set \mathcal{M}_3 , associated to obstacle 3, with an order $\bar{N}_3 = 2$ where the first two obstacles $\mathcal{M}_3^2 = \{4, 1\}$ satisfy conditions 1) and 2) of Lemma 3 while obstacle 2 does not. Our main result in n -dimensional workspaces is stated in the following theorem.

Theorem 1. Consider the free space $\mathcal{F} \subset \mathbb{R}^n$ described in (6), for $n \geq 2$, and the closed-loop system (10)-(24). Under Assumptions 1 and 2, the following statements hold:

- i) The set \mathcal{F} is forward invariant.
- ii) All trajectories converge to the set $\zeta = \{x_d\} \cup (\cup_{i \in \mathcal{Z}} \mathcal{L}_i)$.
- iii) The set of equilibrium points $\cup_{i \in \mathcal{Z}} \mathcal{L}_i$ is unstable.
- iv) The equilibrium point x_d is locally exponentially stable on \mathcal{F} .

³For simplicity, the arguments (x, u) for the angles β_i and θ_i are omitted whenever clear from context.

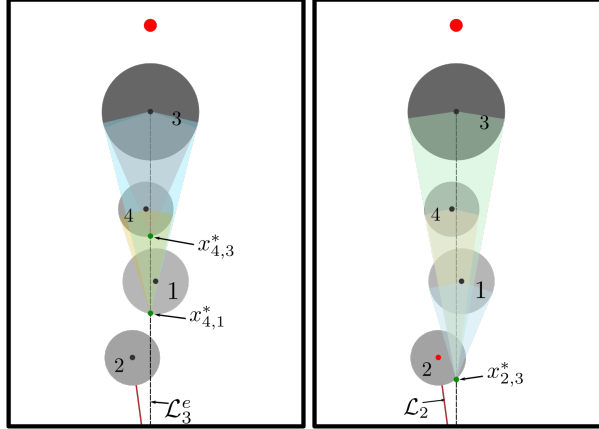


Figure 5: The left figure shows that the obstacles $\{4, 1\}$ satisfies the conditions in Lemma 5 and do not generate undesired equilibria. The right figure shows that obstacle 2 does not satisfy the conditions of Lemma 5 and generates undesired equilibria. The order of the set \mathcal{M}_3 is $\bar{N}_3 = 2$.

v) All trajectory $x(t)$ such that $\lim_{t \rightarrow +\infty} x(t) = x_d$ is generated by a quasi-optimal obstacle avoidance maneuver.

Proof. See Appendix 9. □

Theorem 1 shows that the desired equilibrium point x_d is locally exponentially stable and that all trajectories converging to it are safe and quasi-optimal, in the sense of Definition 1. The region of attraction of the desired equilibrium is characterized in the next section for two-dimensional workspaces. Unfortunately, for higher dimensions, a complete characterization of the region of attraction has not been proved although we claim it is almost global (equivalently, the region of attraction of the undesired equilibria has measure zero).

6.1 Invariant sets in two-dimensional spaces ($n = 2$)

Let $\mathcal{R}_i := \{k \in \mathbb{Z} | \mathcal{L}_k^e \cap \mathcal{O}_i \neq \emptyset, \mathcal{L}_k \cap \mathcal{AR}_i \neq \emptyset\}$ be the set of indices of central half-lines crossing obstacle i and their set of undesired equilibria intersecting with its active region \mathcal{AR}_i , and note that $\mathcal{R}_i \neq \emptyset$ for all $i \in \mathbb{I}$. Obstacles crossed by more than one central half-line are represented by the set of indices $\mathbb{L} := \{k \in \mathbb{I} | \text{card}(\mathcal{R}_k) \geq 2\}$. For every $i \in \mathbb{L}$, we select the out-most line segments \mathcal{L}_k , $k \in \mathcal{R}_i$, and we determine their intersection with the boundary of obstacle i , the left and right intersections being denoted by $y_{i,0}^l$ and $y_{i,0}^r$ respectively. We go through the two out-most line segments separately until they intersect with one of the line segments having an index in the set \mathcal{R}_i , or with the boundary of the workspace. We denote the left and right intersections by y_1^l and y_1^r , respectively. If the workspace has yet to be reached and $(y_1^l \neq y_1^r)$, we continue in the same way with the new line segments up to the intersection with the workspace boundary or up to the intersection between the left and right line segments (*i.e.*, $y_k^l = y_j^r$, $k, p > 0$). We group the intersection points obtained on the left and right into two lists, $Y_i^l = \{y_{i,0}^l, y_{i,1}^l, \dots\}$ and $Y_i^r = \{y_{i,0}^r, y_{i,1}^r, \dots\}$, respectively (see Fig. 6). For every two successive points $\{y_{i,p}^l, y_{i,p+1}^l\}$ of Y_i^l (*resp.* $\{y_{i,p}^r, y_{i,p+1}^r\}$ of Y_i^r), we generate the right (*resp.* left) half-plane bounded by the line passing through these two points. The intersection of the union of the half-planes of each list forms an area that, when restricted to the active region, gives a characteristic region defined as $\chi_i := \left(\bigcup_{p=0}^{\text{card}(Y_i^r)-2} \mathcal{P}_{\geq}^l(y_{i,p}^r, R(y_{i,p}^r - y_{i,p+1}^r)) \right) \cap \left(\bigcup_{p=0}^{\text{card}(Y_i^l)-2} \mathcal{P}_{\leq}^l(y_{i,p}^l, R(y_{i,p}^l - y_{i,p+1}^l)) \right) \cap \mathcal{AR}_i$ where $R = \begin{pmatrix} 0 & 1 \\ -1 & 0 \end{pmatrix}$. Finally, we create a cell, deleting the characteristic regions of other obstacles inside the characteristic region of obstacle i , and define it as follows $\mathbf{Cell}_i := \chi_i \setminus \bigcup_{k \in \mathbb{L}_i} \chi_k$ where $\mathbb{L}_i := \{k \in \mathbb{L} | \chi_i \cap \chi_k \neq \emptyset; \forall x \in \chi_i \cap \chi_k, \iota_x^{-1}(k) > \iota_x^{-1}(i)\}$. Note that the construction of these cells requires their boundaries to be formed by undesired equilibria and the boundary of the free space, which endows them with the invariance property stated in the following lemma.

Lemma 6. Let $i \in \mathbb{L}$. The cell \mathbf{Cell}_i is forward invariant for the closed-loop system (10)-(24).

Proof. See Appendix 9. □

Lemma 7. The set $\bigcup_k \mathbf{Nest}_k$ is the region of attraction of the undesired equilibria $\bigcup_{i \in \mathbb{Z}} \mathcal{L}_i$.

Proof. See Appendix 9. □

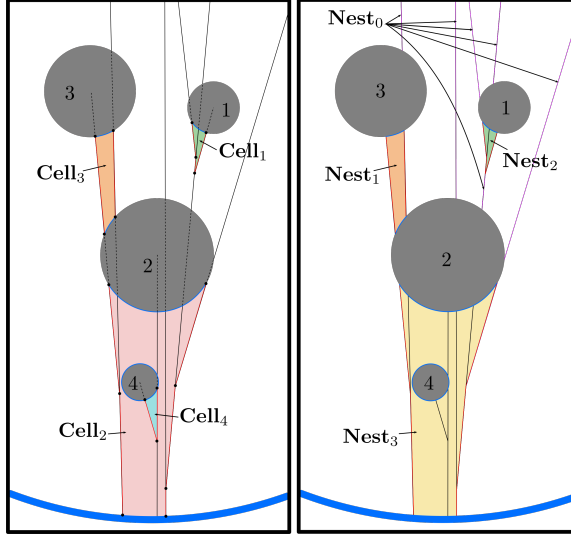


Figure 6: Invariant cells and nests

Two cells are adjacent if they share undesired equilibria on their boundary, which is true only if $\partial\mathbf{Cell}_i \cap \partial\mathbf{Cell}_k \cap (\cup_{i \in \mathcal{Z}} \mathcal{L}_i) \neq \emptyset$. We construct nests by the union of adjacent cells, where each cell has at least one adjacent cell among the cells in that nest. Cells without adjacent cells form a nest with a single element. We also construct a special nest whose cells are segments of undesired equilibria that belong to no other regular cell. Since nests are the union of invariant cells or of undesired equilibria (the special nest), nests are invariant and are denoted by \mathbf{Nest}_k where $\mathbf{Nest}_0 := \cup_{i \in \mathcal{Z}} \mathcal{L}_i \setminus \cup_{k \in \mathbb{L}} \mathbf{Cell}_k$ is the special nest (see Fig. 6). Unfortunately, a nest can form a barrier around the workspace, reducing the navigable area of the free space. Such a nest can be generated by creating a circular band of adjacent cells, as shown in Fig. 7. In the following lemma, nests are shown to be the attraction region of the undesired equilibria.

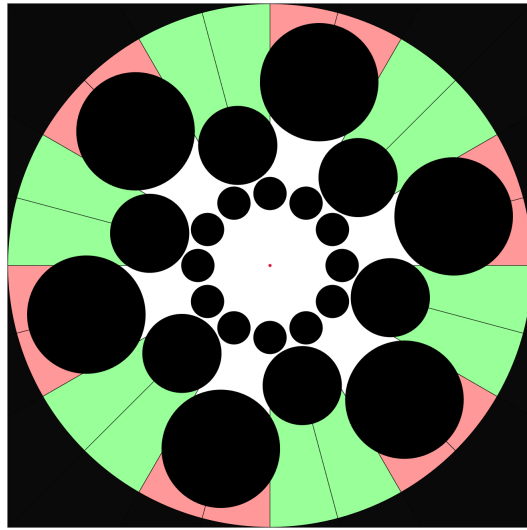


Figure 7: Quasi-non-navigable two-dimensional space.

Now, to ensure almost global asymptotic stability of the equilibrium point x_d in two-dimensional spaces, we reduce the nests to the set of undesired equilibria by imposing the following assumption:

Assumption 3. For any $i \in \mathbb{I}$ and $k \in \mathcal{Z}$ where $i \neq k$, $\mathcal{L}_k^e \cap \mathcal{O}_i = \emptyset$, or $(\mathcal{L}_k^e \cap \mathcal{O}_i \neq \emptyset \text{ and } i \in \mathcal{M}_k^{\bar{N}_i})$.

Assumption 3 rules out the possibility of creating the invariant cells by imposing obstacle configurations such that $\mathbb{L} = \emptyset$ making the undesired equilibria repellers. In addition to the results of Theorem 1, the next theorem characterizes the attraction region of the undesired equilibria and shows almost global asymptotic stability of the destination under Assumption 3.

Theorem 2. Consider the free space $\mathcal{F} \subset \mathbb{R}^n$ described in (6), for $n = 2$, and the closed-loop system (10)-(24). Under Assumptions 1 and 2, items i), ii), iii), iv) of Theorem 1, the following statements hold:

- i) The equilibrium point x_d is attractive from all $x(0) \in \mathcal{F} \setminus \cup_k \text{Nest}_k$.
- ii) From any initial position $x(0) \in \mathcal{F} \setminus \cup_k \text{Nest}_k$, the trajectory $x(t)$ is generated by a quasi-optimal obstacle avoidance maneuver.
- iii) Under Assumption 3, $\cup_k \text{Nest}_k = \cup_{i \in \mathcal{Z}} \mathcal{L}_i$ and the destination x_d is almost globally asymptotically stable.

Proof. See Appendix 9. □

Theorem 2 shows the attraction of the target location from any location in the free space, with the exception of the attraction region of the undesired equilibria, which can be a set of measure zero under Assumption 3 where it reduces to the undesired equilibria $\cup_{i \in \mathcal{Z}} \mathcal{L}_i$. Fortunately, the nests will naturally disappear in the sensor-based case as we will see in the next section.

7 Sensor-based navigation using a 2D LiDAR range scanner

We now present a more practical version of our approach using a LiDAR range scanner in an unknown two-dimensional sphere world. Assume that the robot is equipped with a sensor of 360° angular sensing range, a resolution $d\theta > 0$, and a radial sensing range $R > 0$. The measurements of the sensor, at a position x , are modeled by the polar curve $\rho(x, \theta) : \mathcal{F} \times \hat{\mathcal{A}} \rightarrow [0, R]$, where $\hat{\mathcal{A}} := \{0, d\theta, 2d\theta, \dots, 360 - d\theta\}$ is the set of scanned angles, defined as follows:

$$\rho(x, \theta) := \min \left(R, \frac{\min_{\substack{y \in \partial \mathcal{F} \\ \text{atan2}(y-x)=\theta}} \|x - y\|}{\text{atan2}(y-x)=\theta} \right), \quad (27)$$

where $\overline{\text{atan2}}(v) = \text{atan2}(v(2), v(1))$ for $v \in \mathbb{R}^2$.

The Cartesian coordinates of the scanned points are modeled by the mapping $\delta(x, \theta) : \mathcal{F} \times \hat{\mathcal{A}} \rightarrow \mathcal{F}$ defined as follows:

$$\delta(x, \theta) := x + \rho(x, \theta) [\cos(\theta) \ \sin(\theta)]^\top. \quad (28)$$

Let $G_x(\delta)$ be the graph of the mapping δ at a position x (red curve in Fig. 8). The set $\mathbb{I}_x \subset \mathbb{I}$ of the detected obstacles is defined as $\mathbb{I}_x := \{i \in \mathbb{I} \mid d(x, \mathcal{O}_i) \leq R\}$. Assume that at each position x , the sensor returns a list of arcs $\mathcal{LA}(x) := \{L_1, L_2, \dots, L_{\tau(x)}\}$ from the detected obstacles corresponding to the intersection of the graph $G_x(\delta)$ and obstacles of the set \mathbb{I}_x , where $\tau(x) = \text{card}(\mathbb{I}_x)$ as shown in Fig. 8a by the magenta arcs. Since the available information about the environment is limited by the graph $G_x(\delta)$, successive projections are impossible to apply. Therefore, we apply the single obstacle control strategy given by

$$u(x) = \begin{cases} u_d(x), & x \in \mathcal{VI}, \\ u_d(x) - \|u_d(x)\| \frac{\sin(\theta_i - \beta_i)}{\sin(\theta_i)} V_{ci}, & x \in \mathcal{D}(x_d, c_i), \end{cases}$$

where θ_i and $V_{ci} = (c_i - x)/\|c_i - x\|$ are, respectively, the aperture and the axis of the enclosing cone, β_i is the angle between u_d and $(c_i - x)$, and $\mathcal{D}(x_d, c_i)$ is the shadow region. To adapt the above control strategy to the sensor-based case, one proceeds as follows. At each position x , the detected arcs $\mathcal{LA}(x)$ are considered as obstacles. The arc crossed by the segment $\mathcal{L}(x, x_d)$ will help to create a virtual enclosing cone onto which the projection is performed. However, due to the practical model of the sensor, which may have low resolutions, safety is not always guaranteed when the robot is in the neighborhood of the obstacles where the velocity vector (projection of u_d onto the virtual enclosing cone) may point inside the obstacle (see Fig. 9a). To overcome this problem, a list of extended arcs $\mathcal{LA}_e(x) := \{\tilde{L}_1, \tilde{L}_2, \dots, \tilde{L}_{\tau(x)}\}$ is defined, where the endpoints of an arc L_i are moved through the graph $G_x(\delta)$ until they have a radial polar coordinate equal to R or they meet the endpoints of the neighboring arcs, as shown in Fig. 8b. Among the extended arcs of the list $\mathcal{LA}_e(x)$, the active extended arc crossed by the segment $\mathcal{L}(x, x_d)$ is selected and denoted by \tilde{L}^* . The active extended arc serves as an obstacle enclosed by a virtual cone (see Fig. 8b) from which we extract the following practical parameters:

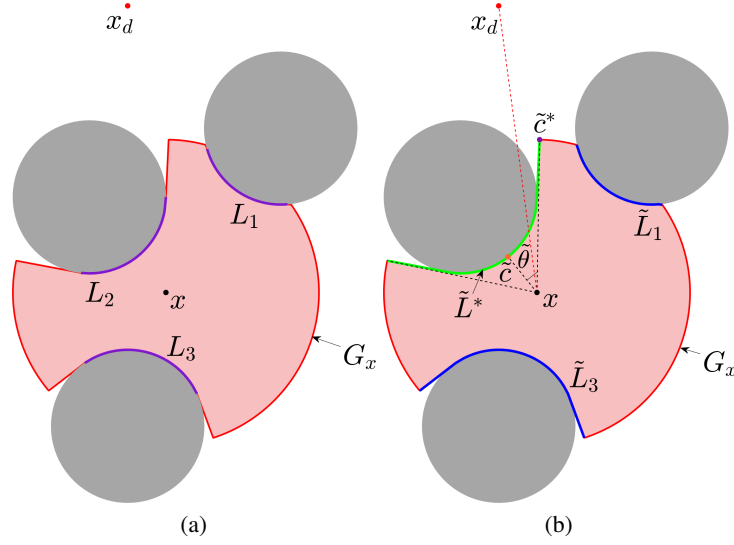


Figure 8: Sensor-based control procedure for our approach.

- The virtual center

$$\tilde{c} := \arg \min_{y \in \tilde{L}^*} \|x - y\|, \quad (29)$$

which gives the direction $(\tilde{c} - x)$.

- The virtual aperture

$$\tilde{\theta} := \angle(\tilde{c} - x, \tilde{c}^* - x), \quad (30)$$

where \tilde{c}^* is an endpoint of \tilde{L}^* such that u_d is between the directions $(\tilde{c} - x)$ and $(\tilde{c}^* - x)$.

- The angle

$$\tilde{\beta} := \angle(\tilde{c} - x, u_d). \quad (31)$$

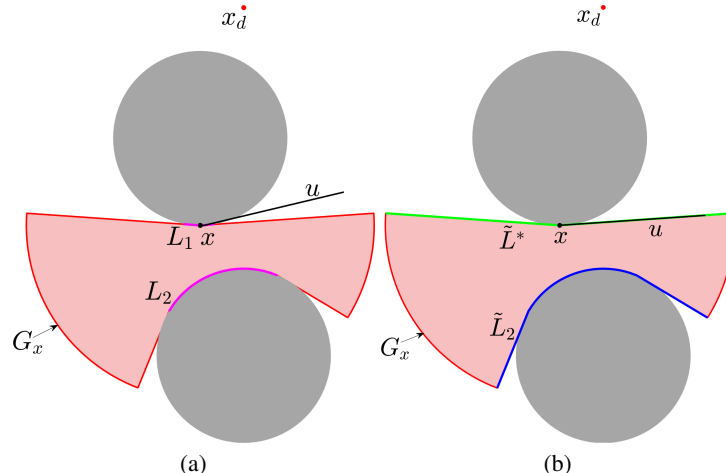


Figure 9: Safety consideration in a sensor-based case. In Fig. (a), the projection u of $(x_d - x)$ onto the cone enclosing the arc L_1 of the list $\mathcal{LA}(x)$ fails to satisfy the safety condition where u crosses the obstacle. In Fig. (b), the projection lies on the active arc \tilde{L}^* of the list $\mathcal{LA}_e(x)$ and meets the safety condition.

Before defining the new blind and visible sets, let us define the truncated shadow region by

$$\mathcal{D}^t(x_d, c_i) := \mathcal{D}(x_d, c_i) \setminus \bigcup_{j \in \mathcal{PR}_i} \mathcal{D}(x_d, c_j), \quad (32)$$

where $\mathcal{PR}_i := \{j \in \mathbb{I} | \mathcal{D}(x_d, c_i) \cap \mathcal{D}(x_d, c_j) \neq \emptyset, d(x_d, \mathcal{O}_i) < d(x_d, \mathcal{O}_j)\}$ is the **progeny** of obstacle i (see Fig. 10a). Since the visibility of the robot is limited to the scanning range of the sensor, let us define the practical shadow region of an obstacle i as follows:

$$\tilde{\mathcal{D}}(x_d, c_i, R) := \mathcal{D}^t(x_d, c_i) \cap \mathcal{B}(c_i, r_i + R). \quad (33)$$

Therefore, the practical blind set is defined as follows:

$$\widetilde{\mathcal{BL}} := \bigcup_{i \in \mathbb{I}} \tilde{\mathcal{D}}(x_d, c_i, R), \quad (34)$$

The practical visible set is then defined as $\widetilde{\mathcal{VL}} := \widetilde{\mathcal{BL}}^c$ (see Fig. 10b). Finally, the control is given by

$$u(x) = \begin{cases} u_d(x), & x \in \widetilde{\mathcal{VI}}, \\ u_d(x) - \|u_d(x)\| \frac{\sin(\tilde{\theta} - \beta)}{\sin(\tilde{\theta})} \frac{\tilde{c} - x}{\|\tilde{c} - x\|}, & x \in \widetilde{\mathcal{BL}}. \end{cases} \quad (35)$$

The implementation of the sensor-based control strategy is summarized in Algorithm 3 (see also Fig. 8).

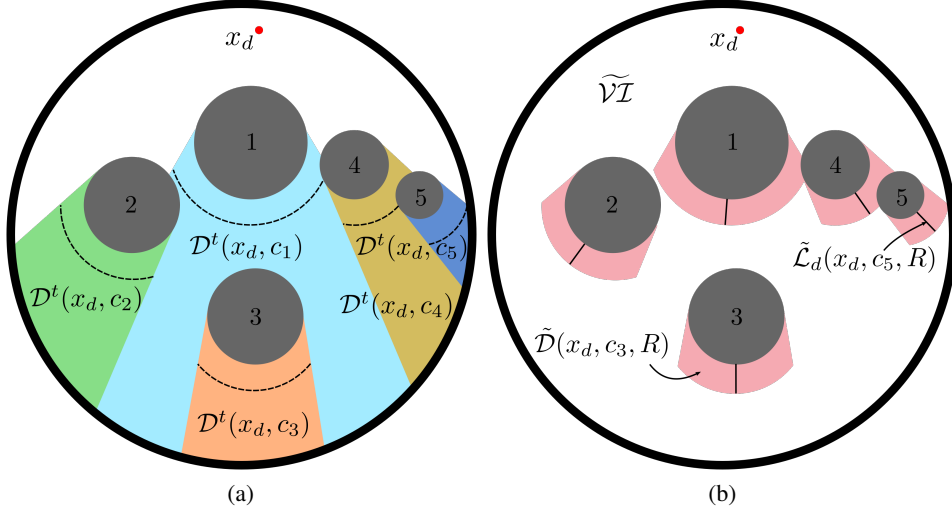


Figure 10: Illustration of the workspace for the sensor-based case. Fig. (a) shows the truncated shadow regions of each obstacle where obstacles $\{2, 3, 4\}$ are the progeny of obstacle 1, and obstacle $\{5\}$ is the progeny of obstacle 4. Fig. (b) highlights the practical shadow regions of each obstacle in pink where the union of these regions represents the practical blind set while the white region represents the practical visible set.

The sensor-based control strategy (35) can be seen as a special case of the control strategy in the map-based scenario (*a priori* known environments) if all obstacles are considered first-generation obstacles. In this way, the active regions become the disjoint practical shadow regions that will limit the undesired equilibria generated by each obstacle to its own practical shadow region excluding the possibility of creating invariant cells. The following lemma determines the equilibria of the closed-loop system (10)-(35) and shows that the undesired equilibria are the sets \mathcal{L}_i restricted to the practical shadow regions.

Lemma 8. *All trajectories of the closed-loop system (10)-(35) converge to the set $\zeta = \{x_d\} \cup \left(\bigcup_{i \in \mathbb{I}} \tilde{\mathcal{L}}_d(x_d, c_i, R) \right)$ where $\tilde{\mathcal{L}}_d(x_d, c_i, R) := \mathcal{L}_d(x_d, c_i) \cap \tilde{\mathcal{D}}(x_d, c_i, R)$ and $\mathcal{L}_d(x_d, c_i) = \mathcal{L}_i$.*

Proof. See Appendix 9. □

The next theorem states formally the properties the sensor-based control strategy in two-dimensional sphere words.

Algorithm 3 Implementation of the control law (35) at an instant t

Input: $x(t), G_x(\delta), \mathcal{LA}(x)$.
Output: u .

```

1: if  $\mathcal{LA}(x) \neq \emptyset$  then
2:   Construct  $\mathcal{LA}_e(x)$ .
3:   if  $\mathcal{L}(x_d, x)$  crosses one of the extended arcs of  $\mathcal{LA}_e(x)$  then
4:     Identify  $\tilde{L}^*$ .
5:     Determine  $\tilde{c}$ ,  $\tilde{\theta}$  and  $\tilde{\beta}$  using equations (29), (30) and (31), respectively.
6:      $u \leftarrow u_d(x) - \|u_d(x)\| \frac{\sin(\tilde{\theta} - \tilde{\beta})}{\sin(\tilde{\theta})} \frac{\tilde{c} - x}{\|\tilde{c} - x\|};$ 
7:   else
8:      $u \leftarrow u_d;$ 
9:   end if
10: else
11:    $u \leftarrow u_d;$ 
12: end if
13: return  $u$ 
```

Theorem 3. Consider the free space $\mathcal{F} \subset \mathbb{R}^n$ described in (6), for $n = 2$, and the closed-loop system (10)-(35). Under Assumptions 1 and 2, the following statements hold:

- i) The set \mathcal{F} is forward invariant.
- ii) All trajectories converge to the set $\zeta = \{x_d\} \cup \left(\cup_{i \in \mathbb{I}} \tilde{\mathcal{L}}_d(x_d, c_i, R) \right)$.
- iii) The set of undesired equilibria $\cup_{i \in \mathbb{I}} \tilde{\mathcal{L}}_d(x_d, c_i, R)$ is unstable.
- iv) The equilibrium point x_d is almost globally asymptotically stable on \mathcal{F} .

Proof. See Appendix 9. □

Theorem 3 provides the stability results obtained with the reactive sensor-based feedback control strategy relying only on local information provided by the sensor, which is more practical and realistic than the global approach, which requires *a priori* knowledge of the entire environment. Admittedly, we lose the continuity guarantees of the control input and the high likelihood of generating optimal trajectories to the benefit of achieving almost global asymptotic stabilization of the target location without restricting the obstacle configurations as per Assumption 3. Fig. 11 shows an example of a discontinuity in our control at time $t = t'$ when the active arc \tilde{L}^* passed from one obstacle to another, resulting in a sudden change in the control's direction to follow the tangent of the new obstacle.

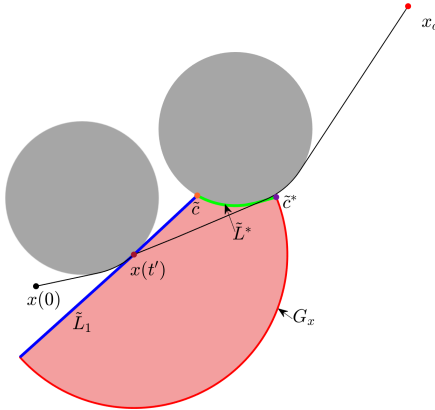


Figure 11: A scenario of a discontinuity occurrence in a 2D workspace populated by two obstacles at time $t = t'$.

7.1 Convex obstacles

We consider convex sets with smooth boundaries $\tilde{\mathcal{O}}_i$ as obstacles. The free space must satisfy the separation conditions of Assumptions 1 and 2. We also assume that the following curvature condition (see, e.g., [Arslan and Koditschek, 2019]) is satisfied.

Assumption 4. *Obstacles are sufficiently curved at their farthest point from the target location $x_d \in \mathcal{F}$, i.e.,*

$$\tilde{\mathcal{O}}_i \subset \mathcal{B}(x_d, \|x_d - \mathbf{x}_i\|), \forall i \in \mathbb{I}, \quad (36)$$

where $\mathbf{x}_i \in \left\{ q \in \partial \tilde{\mathcal{O}}_i \mid d s_i(q)^\top (x_d - q) / \|x_d - q\| = 1 \right\}$, and $d s_i(q) \in \mathbb{S}^{n-1}$ is the inward-directed gradient of the surface of obstacle $\tilde{\mathcal{O}}_i$ at position $q \in \partial \tilde{\mathcal{O}}_i$.

Assumption 4 somewhat limits the flatness of an obstacle at its farthest point from the target, as illustrated in Figure 12. The shadow region for a convex obstacle is redefined as $\mathcal{D}(x_d, i) := \left\{ q \in \mathcal{F} \mid \mathcal{L}(x_d, q) \cap \tilde{\mathcal{O}}_i \neq \emptyset \right\}$, where the center is replaced by the index of the obstacle as a parameter (see Fig. 12). The practical shadow region is then defined as $\tilde{\mathcal{D}}(x_d, i, R) := \left\{ q \in \mathcal{D}^t(x_d, i) \mid d(q, \tilde{\mathcal{O}}_i) \leq R \right\}$, where $\mathcal{D}^t(x_d, i)$ is the truncated shadow region defined in (32), substituting the center with the obstacle's index. The practical parameters and the control are the same as in (35). The next lemma provides the set of equilibria of the closed-loop system (10)-(35) in the case of convex obstacles.

Lemma 9. *All trajectories of the closed-loop system (10)-(35) converge to the set $\tilde{\zeta} = \{x_d\} \cup \left(\cup_{i \in \mathbb{I}} \tilde{\mathcal{L}}_d(x_d, \mathbf{x}_i, R) \right)$, where $\tilde{\mathcal{L}}_d(x_d, \mathbf{x}_i, R) := \mathcal{L}_d(x_d, \mathbf{x}_i) \cap \tilde{\mathcal{D}}(x_d, i, R)$.*

Proof. See Appendix 9. □

In addition to the destination, Lemma 9 shows that the equilibrium points are the positions aligned with their projection \tilde{c} and the destination. The same sensor-based procedure applied in sphere worlds is used, except that the elements of the

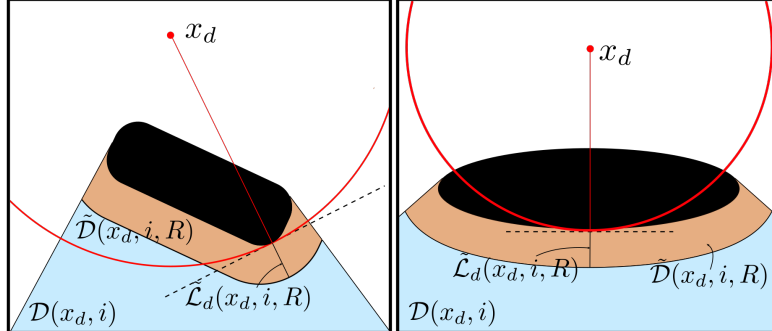


Figure 12: Representation of the shadow region and the practical shadow region of a convex obstacle. In the figure on the left, the obstacle satisfies the curvature condition, while in the figure on the right, the obstacle does not satisfy this condition.

list of arcs are not arcs but convex portions of the detected obstacles. In the case of convex obstacles with non-smooth boundaries, the procedure is modified where the endpoints of each detected portion are dilated with a ball of radius $r > 0$, and the cone enclosing the segment crossed by $\mathcal{L}(x, x_d)$ is enlarged, as shown in Fig. 13. The objective of dilating the endpoints is to smooth the corners of the obstacles. When an endpoint coincides with the vertex of an obstacle, the dilated endpoint will help to generate a smooth trajectory. If the robot rotates around an obstacle and applies the endpoint dilation on its boundary, a diluted version of this obstacle, given by $\tilde{\mathcal{O}}_i^r = \tilde{\mathcal{O}}_i \oplus \mathcal{B}(0, r)$, will be generated. Therefore, the new free space will be $\mathcal{F}_r := \mathcal{W} \setminus \bigcup_{i=1}^m \tilde{\mathcal{O}}_i^r$ and the minimum separation distance will be greater than $2r$.

Theorem 4. *Consider the free space $\mathcal{F} \subset \mathbb{R}^n$ described in (6), in the case of convex obstacles and $n = 2$, and the closed-loop system (10)-(35). Under Assumptions 1, 2, and 4, the following statements hold:*

- i) *The set \mathcal{F} is forward invariant.*

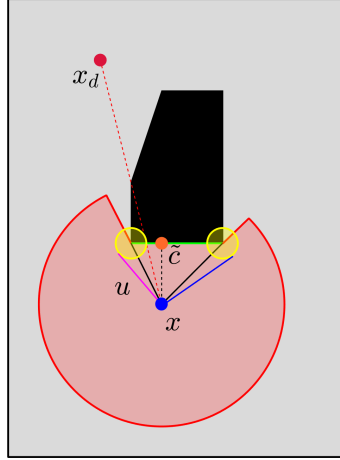


Figure 13: Smoothing of polygonal obstacle corners.

- ii) All trajectories converge to the set $\tilde{\zeta} = \{x_d\} \cup \left(\bigcup_{i \in \mathbb{I}} \tilde{\mathcal{L}}_d(x_d, \mathbf{x}_i, R) \right)$.
- iii) The set of undesired equilibria $\bigcup_{i \in \mathbb{I}} \tilde{\mathcal{L}}_d(x_d, \tilde{\mathbf{x}}_i, R)$ is unstable.
- iv) The equilibrium point x_d is almost globally asymptotically stable on \mathcal{F} .

Proof. See Appendix 9. □

Theorem 4 shows that the sensor-based strategy designed for sphere worlds extends to convex worlds with obstacles satisfying the curvature condition of Assumption 4, and the results are preserved. For convex obstacles with non-smooth boundaries, we consider their dilated version $\tilde{\mathcal{O}}_i^r$ and the free space \mathcal{F}_r which amounts to the case of obstacles with smooth boundaries.

8 Numerical simulation

8.1 A priori known sphere worlds

To explore the extent of what our quasi-optimal avoidance maneuver can offer in terms of the shortest path in the multiple obstacle case, we compare the trajectories of our method to the shortest paths obtained with Dijkstra's algorithm (DA) on a visibility tangent graph in ten different and highly congested two-dimensional spaces shown in Fig. 14. In each space, 100 random initial conditions are taken, and the number of perfect matching of the paths is determined. A simulation video of Fig. 145 can be found at <https://youtu.be/SE8w8vabxE>. The summarized results in Table 1 show a high rate of success, while the failures of taking the shortest path can be explained by the fact that, at each position x , our algorithm performs $h(x)$ nested projections with respect to the obstacles of the set $\mathcal{I}(x)$ that may lead to a non-optimal path. Compared to Dijkstra's algorithm, which takes the shortest path from all possible paths of the visibility tangent graph. Fig. 21 illustrates the effect of the imbrication of the projections on generating the shortest path. In Fig. 15a, the path generated by our approach coincides with the DA path in a single obstacle workspace. In contrast, in Fig. 15b, our approach generates a non-optimal path in a two-obstacle workspace.

Table 1: Success rate of the perfect match between the paths generated by our control strategy and the paths of DA.

Space 1	Space 2	Space 3	Space 4	Space 5
100%	98%	100%	100%	81%
Space 6	Space 7	Space 8	Space 9	Space 10
96%	99%	94%	94%	99%

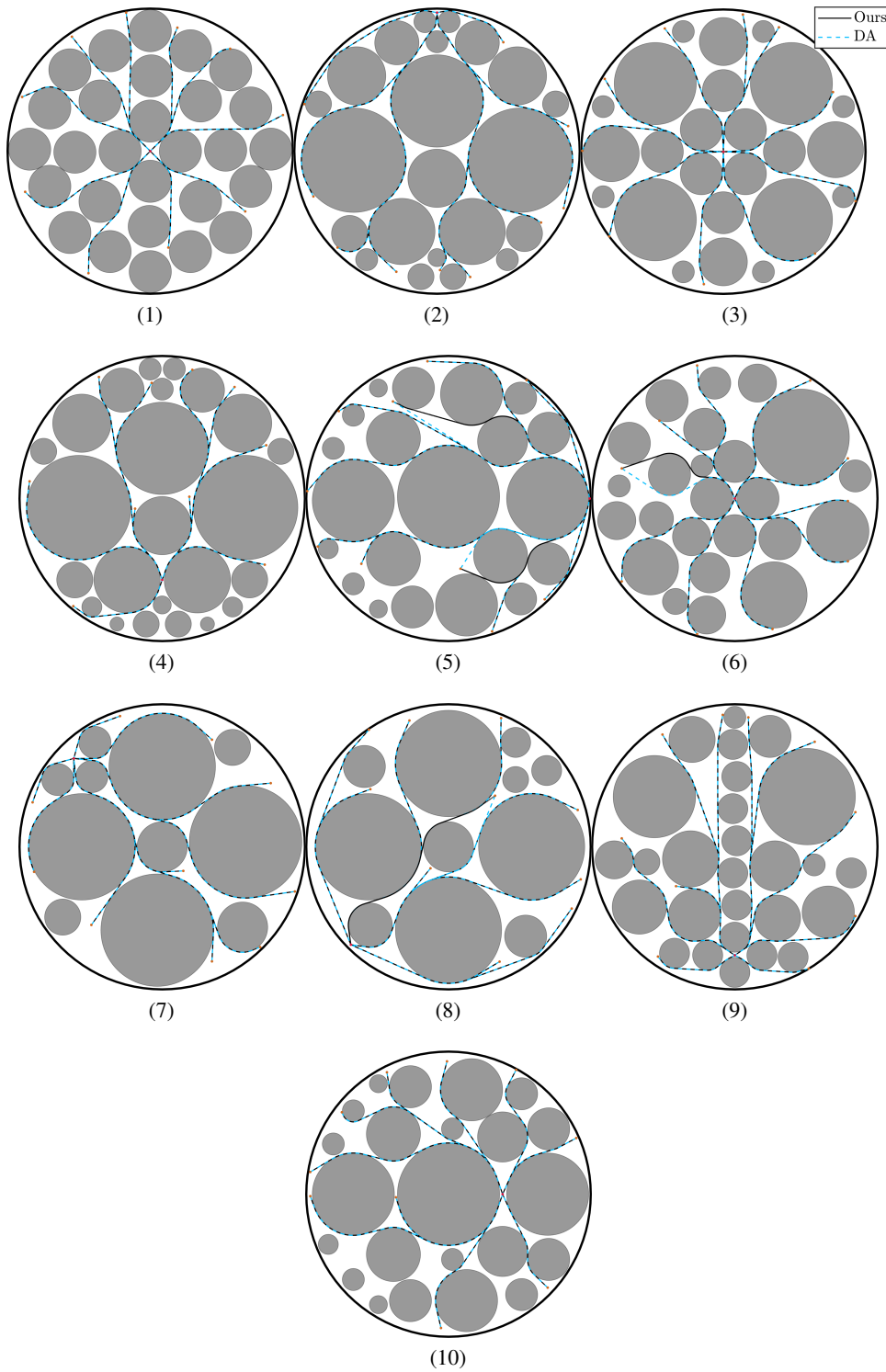


Figure 14: Some samples among 100 tests between (DA) and our approach in 10 different spaces.

Remark 2. The DA has been used as a benchmark to test the optimality of the paths generated by our approach. The advantages of our approach w.r.t. the DA algorithm are as follows:

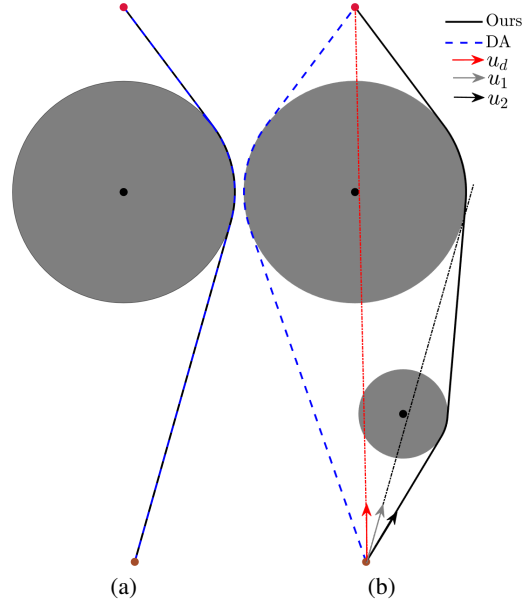


Figure 15: Effect of the nested projections on the optimality of the generated trajectory. In Fig. (a), a single obstacle is considered, and the trajectory generated by our approach corresponds to the DA trajectory. In Fig. (b), a second obstacle is considered. The trajectory generated by our approach differs from the DA trajectory.

- We solve the problem from a control perspective, as our solution is feedback-based, allowing us to solve the navigation problem in one go, whereas DA only gives the shortest path to be tracked by another feedback controller.
- We propose a closed-form solution which is more suitable for real-time implementations (computationally efficient) than searching tangent visibility graphs.
- We solve the navigation problem in an arbitrary n -dimensional sphere world while the DA is limited to paths in two-dimensional worlds as the tangent visibility graph is infinite in higher dimensions.

To visualize the properties of our approach, we consider two different scenarios. In the first scenario, we assume that the robot evolves in \mathbb{R}^2 where the workspace contains twenty-six obstacles, and the destination is $x_d = [0 \ 0]^\top$. We run the simulation from fifteen different initial positions. In the second scenario, the considered space is \mathbb{R}^3 , where the workspace contains eighteen obstacles, and the goal is $x_d = [0 \ 0 \ 0]^\top$. We run the simulation from eighteen different initial positions. A comparison of our approach with the **navigation function approach (NF)** [Koditschek and Rimon, 1990] and the **separating hyperplane approach** with the Voronoi-adjacent obstacle sensing model (**SH**) [Arslan and Koditschek, 2019] is established in the two-dimensional space. The simulation results in Fig. 16 and 17 show that all the trajectories generated by our control strategy are safe and converge to the red target. In addition, Fig. 16 shows the superiority of our approach over the two other methods in terms of the length of the generated collision-free paths, as shown in Table 2, where it generates the same paths as DA. This superiority is mainly due to the uncontrolled repulsion exerted by the obstacles on the robot in the NF and SH approaches. It becomes clear in the single obstacle case where the robot is repelled even if it has a clear line-of-sight to the destination, which is shown in the simulation result in Fig. 18, where the pink initial positions are in the visible set while the green initial positions are in the shadow region. The trajectories generated by our approach are the shortest in terms of distance, as shown in Lemma 1. The simulation video of Fig. 17 can be found at <https://youtube.com/shorts/yJCdRLdQHnc>.

Let us test our control in a two-dimensional space that does not satisfy Assumption 3. We consider six different initial positions. Three are inside the nests, and the remaining three are outside but in the vicinity of their boundaries (undesired equilibria). The results of the simulation are shown in Fig. 19. The trajectories starting from the nests stay inside, while the three remaining trajectories reach their destination safely. We can see that nests are indeed the attraction region of the undesired equilibria.

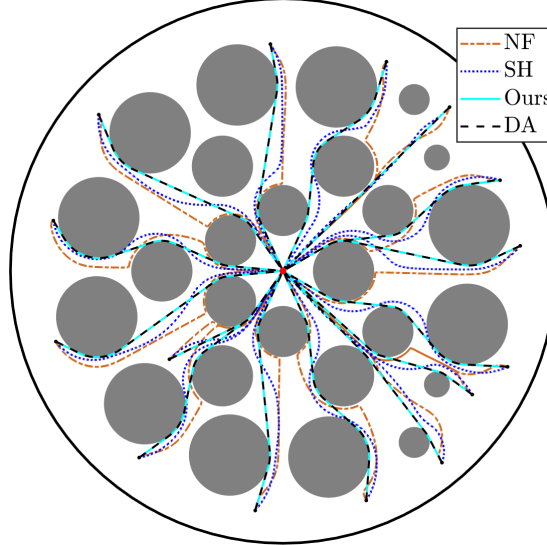


Figure 16: Comparison of paths generated by Our approach, SH, and NF to the paths generated by DA in a two-dimensional sphere world.

Table 2: The error of the length of the trajectories generated by the NF and SH approaches compared to our approach. The error considered for each initial position i (in Fig. 16) is determined by $100(l^i - l_0^i)/l_0$, where l^i is the length of the i th trajectory generated by the SH or NF approach, and l_0 is the length of the trajectory generated by our approach.

Paths	NF	SH
1	1.18%	0.27%
2	11.36%	7.59%
3	8.6%	5.2%
4	5.93%	7.23%
5	6.57%	3.64%
6	4.26%	2.43%
7	13.35%	7.15%
8	6.6%	3.79%
9	11.34%	5.47%
10	6.63%	2.98%
11	9.79%	3.91%
12	14.08%	5.05%
13	9.24%	4.24%
14	7.23%	4.31%
15	4.65%	6.96%

8.2 Sensor-based implementation

8.2.1 MATLAB Simulation

In the same workspace as in Fig. 16, we tested the sensor-based control strategy (35), where the robot starts from twelve different initial positions. Relying on a 360° LiDAR with a 1° resolution, the robot reaches safely the destination (red point) as shown in Fig. 20. The simulation video can be found at <https://youtu.be/cnWoxi-1Gvw>.

To test the proposed sensor-based approach in convex environments, a first simulation in a convex workspace, with ellipsoidal obstacles satisfying the curvature condition of Assumption 4, is run from twelve initial positions. The results in Fig. 21a show the effectiveness of the proposed approach in convex worlds with smooth boundaries where the 12 generated paths are all safe and converge to the target location. The simulation video can be found at <https://youtu.be/Y5dho-ptkm8>. The second simulation is performed in a convex workspace with polygonal obstacles satisfying the curvature condition of Assumption 4 where eleven initial positions are considered. The

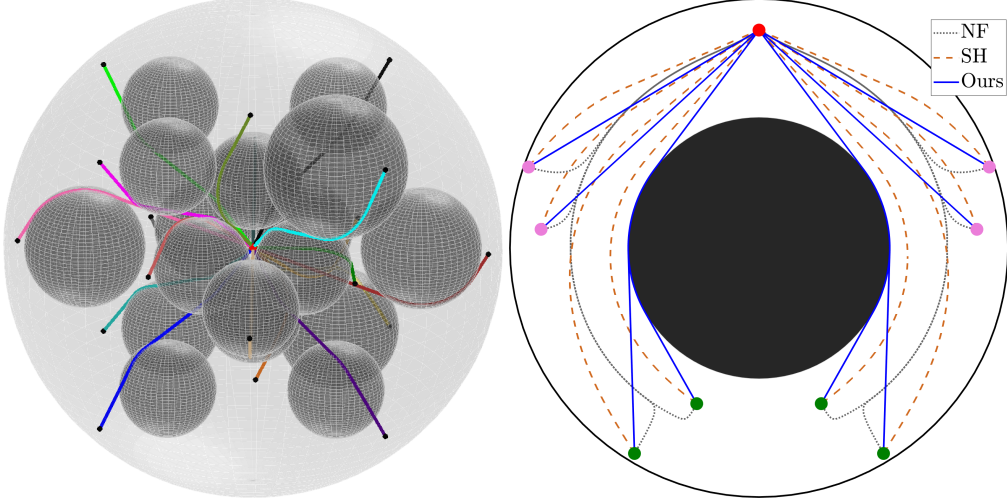


Figure 17: Robot safe navigation from eighteen different initial positions in a three-dimensional world with multiple spheres.
 Figure 18: Comparison of paths generated by our approach, SH, and NF in a single two-dimensional sphere world.

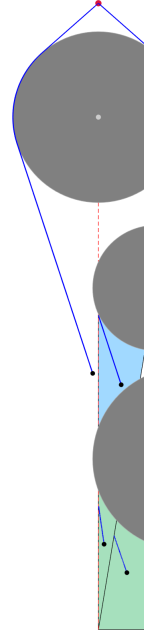


Figure 19: Invariance of the nests.

results in Fig. 21b show the effectiveness of the proposed approach in convex worlds with polygonal obstacles where the 11 generated paths are all safe and converge to the target location. The simulation video can be found at <https://youtu.be/FZ0qxx6Gsog>.

8.2.2 Gazebo simulation

For experimental validation of our sensor-based approach, we used the meta-operating system ROS (Noetic) running on Ubuntu (20.04.6) to implement the control strategy (35) on a Turtlebot3 model and simulate real-world scenarios with Gazebo (3D dynamic simulator). Our code is written in Python, and the data analysis is performed in MATLAB. The TurtleBot model includes a 360° Lidar with a resolution of 1°, a maximum range $R = 3.4\text{ m}$, and a minimum range of 0.12 m. The robot's position and orientation are obtained by subscribing to the odometry topic provided by ROS. Zero mean Gaussian noise is added to the sensors' data where the standard deviation for the Lidar is 0.02 m, the standard

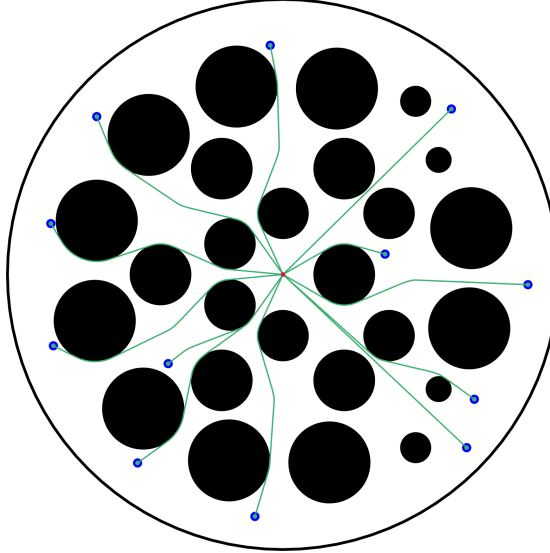


Figure 20: Sensor-based navigation in an unknown 2D sphere world.

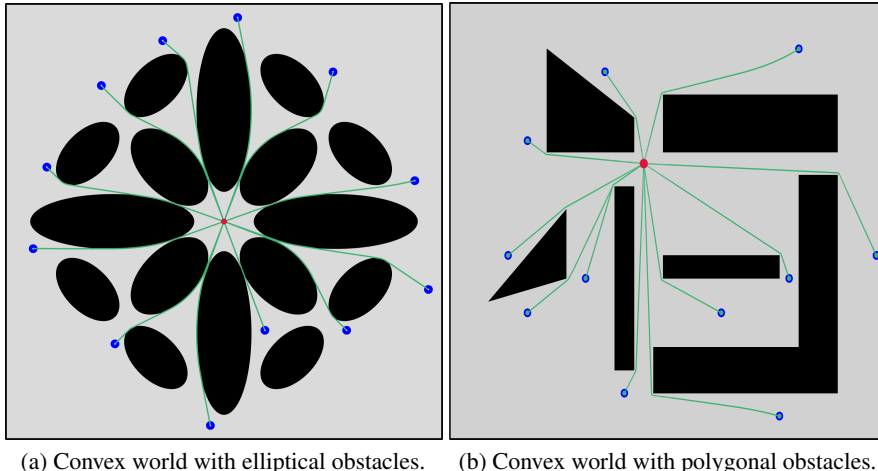


Figure 21: Sensor-based navigation in unknown 2D convex worlds.

deviation for the position is 0.03 m , and for the orientation, the standard deviation is 0.035 rd . As the TurtleBot has a disk-shaped base of radius $r_b = 0.14 \text{ m}$, we consider the eroded workspace $\mathcal{W}_r := \mathcal{W} \setminus (\partial\mathcal{W} \oplus \mathcal{B}(0, r))$, and the dilated obstacles $\tilde{\mathcal{O}}_i^r$. The eroded free space is then defined as $\mathcal{F}_r := \mathcal{W}_r \setminus \cup_{i \in \mathbb{I}} \tilde{\mathcal{O}}_i^r$ and for all $x \in \mathcal{F}_r$, $\mathcal{B}(x, r_b) \subset \mathcal{F}$. Considering that x (the center of the robot's base) evolves in the eroded free space \mathcal{F}_r , and choosing the dilation parameter $r = r_b + r_s$, where $r_s = 0.11 \text{ m}$ is a security margin, the robot is guaranteed to evolve in the free space \mathcal{F} . TurtleBot 3 is a differential drive robot whose kinematic model is represented by

$$\begin{cases} \dot{x} = v[\cos(\psi) \sin(\psi)]^\top, \\ \dot{\psi} = \omega, \end{cases} \quad (37)$$

where $\psi \in (-\pi, \pi]$ is the robot's orientation, and $v \in \mathbb{R}$ and $\omega \in \mathbb{R}$ are, respectively, the robot's linear and angular velocity inputs. As the control law 35 was designed for fully actuated robots, a transformation is required to generate adequate velocity inputs for our robot. The principal idea is to rotate the robot so that its orientation coincides with the direction of $u(x)$ obtained from (35), and then translate the robot with a linear velocity equal to the magnitude of $u(x)$. The direction of $u(x)$ is denoted by $\psi_d = \text{atan2}(u(x))$, and the difference between the robot's orientation and the direction of $u(x)$ is denoted by $\Delta\psi = \psi - \psi_d \in (-\pi, \pi]$. We transform the velocity input of a fully actuated robot to the velocity inputs of a nonholonomic mobile robot with smooth switching between the rotation and translation using

the following transformation (inspired from [Sawant et al., 2023b]):

$$\begin{cases} v = \min \left(v_{max}, k_v \|u(x)\| \cos\left(\frac{\Delta\psi}{2}\right)^{2p} \right), \\ \omega = \omega_{max} \sin\left(\frac{\Delta\psi}{2}\right), \end{cases} \quad (38)$$

where $k_v > 0$, $p \geq 1$, $v_{max} = 0.26 \text{ m/s}$ and $\omega_{max} = 1.82 \text{ rad/s}$ are the maximum supported velocities by the robot's actuators. The higher the exponent $2p$, the safer our robot is, and its trajectory is closer to the one generated by the control (35). We created a Gazebo world cluttered with obstacles whose dilated versions adhere to Assumption 4, and we added non-convex walls facing the destination. In this Gazebo world, we implemented the transformed control law (38) on the TurtleBot 3, where we set the gain to $k_v = 0.8$ and the exponent $p = 3$. The results are shown in Fig. 22, and the simulation video can be found at <https://youtu.be/g1Ya9RFSgJc>.

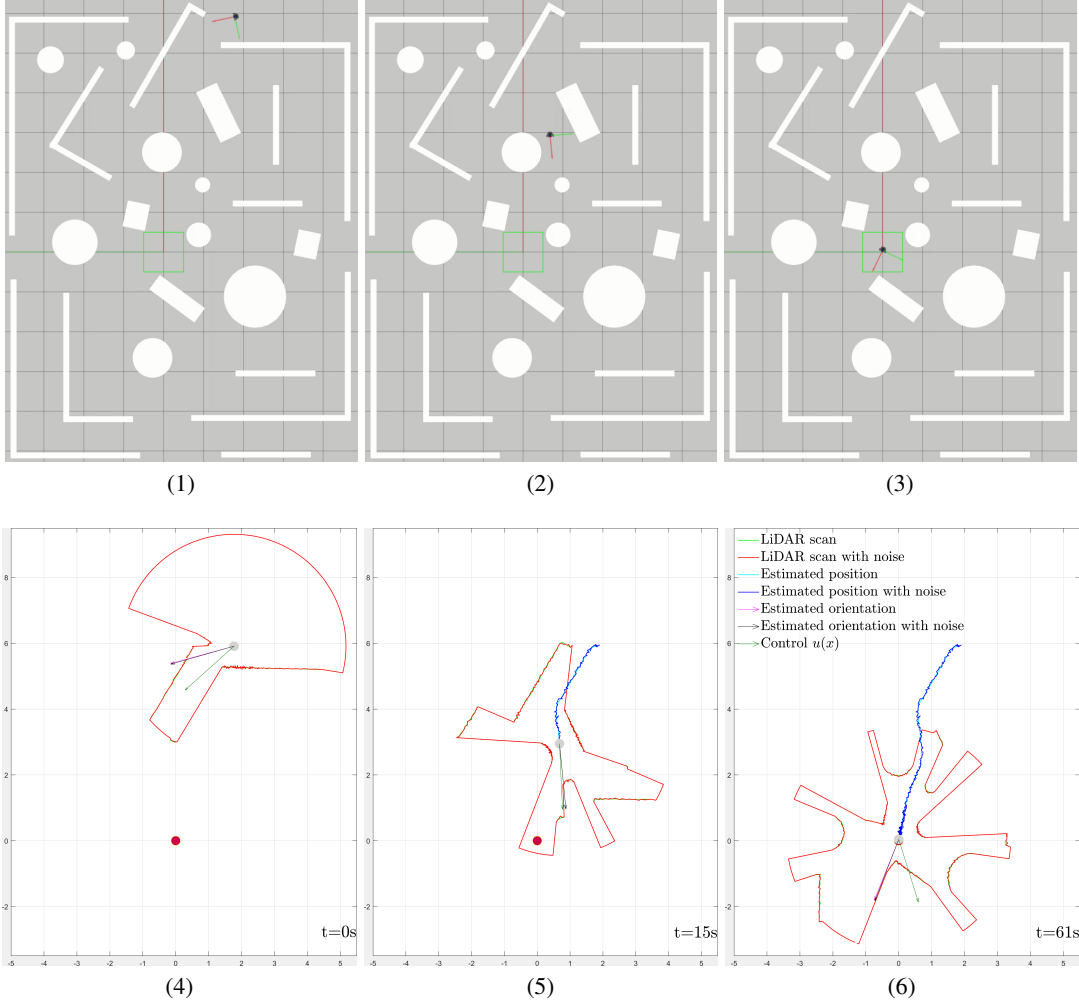


Figure 22: Time-stamped shots of Turtlebot 3 navigating a Gazebo world.

9 Conclusion

A quasi-optimal continuous feedback control strategy, with safety guarantees, for the autonomous navigation problem in an n -dimensional sphere world, has been proposed. The proposed strategy consists in steering the robot tangentially to the blocking obstacles through successive projections of the nominal control onto the obstacles enclosing cones. Consequently, the intermediary obstacle avoidance maneuvers are optimal, resulting in a quasi-optimal overall collision-free path. The price to pay for the almost global asymptotic stability result, in two-dimensional sphere worlds, is

a somewhat restrictive assumption on the configuration of the obstacles (Assumption 3) that has been lifted in the sensor-based version, where the robot can navigate to the target location from almost everywhere in the free space without prior knowledge of environment containing sufficiently curved convex obstacles. Extending the proposed approach to arbitrarily shaped obstacles, with global asymptotic stability guarantees, is another interesting problem that will be the main focus of our future work.

Appendix

Proof of Lemma 1

Minimizing the angle $\angle(x_d - x, v_i)$ is equivalent to minimizing the cost function $g(v_i) = 1 - V_d^\top \frac{v_i}{\|v_i\|}$ with $V_d = (x_d - x)/\|x_d - x\|$ under the constraint $\Gamma(v_i) = \frac{v_i^\top V_{ci}}{\|v_i\|} - \cos(\theta_i) = 0$ with $V_{ci} = (c_i - x)/\|c_i - x\|$. Define the Lagrangian associated to the optimization problem (17) by $L_\lambda(v_i) = g(v_i) - \lambda\Gamma(v_i)$ where λ is the Lagrange multiplier. The optimum is the solution of

$$\nabla_{v_i} L_\lambda(v_i) = 0, \nabla_\lambda L_\lambda(v_i) = 0,$$

which gives

$$\pi^\perp(v_i)(V_d + \lambda V_{ci}) = 0, \quad \frac{v_i^\top V_{ci}}{\|v_i\|} - \cos(\theta_i) = 0. \quad (39)$$

From the first equation, one has $v_i = \alpha(V_d + \lambda V_{ci})$ for some $\alpha \in \mathbb{R}$. Substituting this into the second equation, one gets

$$\alpha(\cos(\beta_i) + \lambda) = \cos(\theta_i)\|\alpha(V_d + \lambda V_{ci})\|. \quad (40)$$

Squaring (40) and substituting $\|\alpha(V_d + \lambda V_{ci})\|^2 = \alpha^2(\lambda^2 + 2\lambda\cos(\beta_i) + 1)$, one can solve for λ

$$\lambda_{1,2} = -\frac{\sin(\theta_i \pm \beta_i)}{\sin(\theta_i)}. \quad (41)$$

Consequently, one can obtain v_i^1 and v_i^2 as follows:

$$v_i^{1,2} = \pm|\alpha| \left(V_d - \frac{\sin(\theta_i \pm \beta_i)}{\sin(\theta_i)} V_{ci} \right). \quad (42)$$

The value of g at the two solutions is as follows:

$$g(v_i^1) = 1 + \cos(\theta_i + \beta_i), \quad g(v_i^2) = 1 - \cos(\theta_i - \beta_i),$$

and $g(v_i^1) - g(v_i^2) = 2\cos(\theta_i)\cos(\beta_i) \geq 0$ which implies that

$$\mathcal{U}_1(x) = \{\bar{\alpha}(V_d - \sin^{-1}(\theta_i)\sin(\theta_i - \beta_i)V_{ci}) \mid \bar{\alpha} \geq 0\}. \quad (43)$$

When $x \in \mathcal{S}(x_d, c_i)$, $u_d(x) \in \mathcal{V}(c_i - x, \theta_i)$ which implies that $\theta_i = \beta_i$, and for all $v_i \in \mathcal{U}_1$, $v_i \in \mathcal{U}_2$. Therefore, $\bar{\alpha}V_d = u_d(x)$ which implies that $\bar{\alpha} = \gamma\|x_d - x\|$. One can conclude that the set $\mathcal{U}_1 \cap \mathcal{U}_2$ is a singleton and the unique solution is given by

$$u(x) = \gamma\|x_d - x\| \left(V_d - \frac{\sin(\theta_i - \beta_i)}{\sin(\theta_i)} V_{ci} \right) = \xi(u_d(x), x, i),$$

where the last equation is obtained after some straightforward manipulations.

Proof of Lemma 2

Let $x(0) \in \mathcal{F} \setminus \mathcal{L}_d(x_d, c_i)$. Then, one has two situations. First, when $x(0) \in \mathcal{VL}$, the trajectory $x(t)$ is a line-segment which is the closest path. Now, when $x(0) \in \mathcal{D}(x_d, c_i)$, there are two types of possible trajectories: trajectories inside the enclosing cone $\mathcal{C}_{\bar{\mathcal{F}}}^<(x, c_i - x, \theta_i)$ and trajectories outside this cone. One can show that the trajectory generated by the closed-loop system (10)-(22), on the enclosing cone $\mathcal{C}_{\bar{\mathcal{F}}}^=(x, c_i - x, \theta_i)$, has minimum length. For the first type of trajectory, one only considers the ones between the line segment $\mathcal{L}(x(0), x_d)$ and the closest tangent to it (green segment in Fig. 23) among the cone enclosing the obstacle (the red trajectory in Fig. 23 is an example). All these trajectories will merge with our trajectory, which is on the closest tangent (as shown in Lemma 1), at the intersection point of the tangent with the obstacle. Since, before the intersection point, our trajectory is a line segment, one can conclude that it is the shortest path. The best that can be achieved outside the cone for a smooth trajectory is a dilated version of our trajectory (larger radius of curvature) which is longer than ours (black path in Fig. 23).

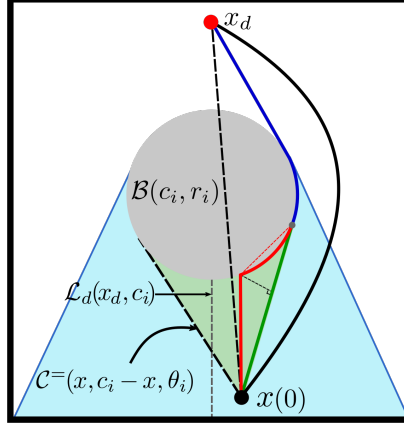


Figure 23: Shortest path in a single-obstacle sphere world.

Proof of Lemma 3

First, we prove that the closed-loop system admits a unique solution. The control is Lipschitz on $\mathcal{V}\mathcal{I}$ since $u(x) = u_d(x)$ is continuously differentiable. When $x \in \mathcal{BL}$, for simplicity, $\sin(\theta_{\iota_x(p)}(q) - \beta_{\iota_x(p)}(u_{p-1}(x), q))$ is denoted by $s_{\iota_x(p)}^s(q)$ and $\frac{\sin(\beta_{\iota_x(p)}(u_{p-1}(x), q))}{\sin(\theta_{\iota_x(p)}(q))}$ by $s_{\iota_x(p)}^d(q)$, where $p \in \{1, \dots, h(x)\}$. After manipulation, the control (24) can be expressed as $u(x) = u_d(x) - \gamma \|x - x_d\| \sum_{p=1}^{h(x)} \prod_{k=1}^{p-1} s_{\iota_x(k)}^d(x) \frac{s_{\iota_x(p)}^s(x)}{r_{\iota_x(p)}} (c_{\iota_x(p)} - x)$, which is shown to be one-sided Lipschitz as follows:

$$\begin{aligned}
(u(x) - u(y))^\top (x - y) &= -\gamma \|x - y\|^2 - \gamma \|x_d - x\| \sum_{p=1}^{h(x)} \prod_{k=1}^{p-1} s_{\iota_x(k)}^d(x) \frac{s_{\iota_x(p)}^s(x)}{r_{\iota_x(p)}} (c_{\iota_x(p)} - x)^\top (x - y) \\
&\quad + \gamma \|x_d - y\| \sum_{p=1}^{h(y)} \prod_{k=1}^{p-1} s_{\iota_x(k)}^d(y) \frac{s_{\iota_x(p)}^s(y)}{r_{\iota_x(p)}} (c_{\iota_x(p)} - y)^\top (x - y), \\
&\leq -\gamma \|x - y\|^2 + \gamma \|x_d - x\| \|x - y\| \sum_{p=1}^{h(x)} \prod_{k=1}^{p-1} s_{\iota_x(k)}^d(x) \frac{s_{\iota_x(p)}^s(x)}{r_{\iota_x(p)}} \|c_{\iota_x(p)} - x\| \\
&\quad + \gamma \|x_d - y\| \|x - y\| \sum_{p=1}^{h(y)} \prod_{k=1}^{p-1} s_{\iota_x(k)}^d(y) \frac{s_{\iota_x(p)}^s(y)}{r_{\iota_x(p)}} \|c_{\iota_x(p)} - y\|.
\end{aligned}$$

Note that $\forall x \in \mathcal{BL}$ and $\forall p \in \{1, \dots, h(x)\}$, $0 \leq s_{\iota_x(p)}^d(x) \leq 1$, $0 \leq s_{\iota_x(p)}^s(x) \leq 1$, $\|c_{\iota_x(p)} - x\| \leq 2r_0 - r_{\iota_x(p)}$ and $\|x_d - x\| \leq 2r_0$, which implies that there exists $M > 0$ such that $\|x_d - x\| \sum_{p=1}^{h(x)} \frac{\|c_{\iota_x(p)} - x\|}{r_{\iota_x(p)}} \leq M \|x - y\|$. Therefore,

$$\begin{aligned}
(u(x) - u(y))^\top (x - y) &\leq -\gamma \|x - y\|^2 + \gamma M_1 \|x - y\|^2 + \gamma M_2 \|x - y\|^2 \\
&\leq \gamma(-1 + M_1 + M_2) \|x - y\|^2 \\
&\leq L \|x - y\|^2.
\end{aligned}$$

One can take $L = \gamma(-1 + M_1 + M_2)$ where $M_1 > 0$, $M_2 > 0$ and $M_1 + M_2 > 1$. The control (24) is one-sided Lipschitz [Cortes, 2008] when $x \in \mathcal{BL}$, and is Lipschitz when $x \in \mathcal{VI}$. Thus, according to [Cortes, 2008, Proposition 2], the closed-loop system (10)-(24) has a unique solution for all $x(0) \in \mathcal{F}$. Now, we prove forward invariance using Nagumo's theorem. We only need to verify Nagumo's condition at the free space boundary as it is trivially met when $x \in \mathring{\mathcal{F}}$ where $\mathcal{T}_{\mathcal{F}}(x) = \mathbb{R}^n$. Since the free space is a sphere world, the tangent cone on its boundary is the half-space $\mathcal{C}_{\mathbb{R}^n}^{\leq}(x, -x, \frac{\pi}{2})$ when $x \in \partial\mathcal{W}$ and $\mathcal{C}_{\mathbb{R}^n}^{\geq}(x, c_i - x, \frac{\pi}{2})$ when $x \in \partial\mathcal{O}_i$ (see Fig. 4). Let us consider an obstacle \mathcal{O}_i and verify Nagumo's condition in three regions of the free space.

In the first region, When $x \in \partial\mathcal{W}$, $\mathcal{T}_{\mathcal{F}}(x) = \mathcal{C}_{\mathbb{R}^n}^{\leq}(x, -x, \frac{\pi}{2})$ and two sub-regions must be considered.

- $x \in \partial\mathcal{W} \cap \partial\mathcal{BL}$ (brown arc in Fig. 4): Since $u(x) \in \mathcal{C}_{\mathcal{F}}^{\leq}(x, c_i - x, \theta_i)$ and $\mathcal{C}_{\mathcal{F}}^{\leq}(x, c - x, \theta) \subseteq \mathcal{C}_{\mathbb{R}^n}^{\leq}(x, -x, \frac{\pi}{2})$, one concludes that $u(x) \in \mathcal{T}_{\mathcal{F}}(x)$.
- $x \in \partial\mathcal{W} \setminus \partial\mathcal{BL}$ (grey arc in Fig. 4): Since $u_d(x) \in \mathcal{F}$ and $\mathcal{F} \subseteq \mathcal{C}_{\mathbb{R}^n}^{\leq}(x, -x, \frac{\pi}{2})$, one concludes that $u(x) = u_d(x) \in \mathcal{T}_{\mathcal{F}}(x)$.

In the second region, $x \in \partial\mathcal{O}_i \cap \mathcal{AR}_i$ (green arc in Fig. 4) and $\mathcal{T}_{\mathcal{F}}(x) = \mathcal{C}_{\mathbb{R}^n}^{\geq}(x, c_i - x, \frac{\pi}{2})$. Since $u(x) \in \mathcal{C}_{\mathbb{R}^n}^{\leq}(x, c_i - x, \frac{\pi}{2}) \subset \mathcal{C}_{\mathbb{R}^n}^{\geq}(x, c_i - x, \frac{\pi}{2})$, one concludes that $u(x) \in \mathcal{T}_{\mathcal{F}}(x)$. Finally, in the last region, $x \in \partial\mathcal{O}_i \setminus \mathcal{AR}_i$ (blue arc in Fig. 4) and $\mathcal{T}_{\mathcal{F}}(x) = \mathcal{C}_{\mathbb{R}^n}^{\geq}(x, c_i - x, \frac{\pi}{2})$. Since $x \notin \mathcal{AR}_i$, $\forall p \in \{0, \dots, h(x)\}$, obstacle \mathcal{O}_i is not selected in the successive projections ($\iota_x(p) \neq i$) and $u_p(x) \notin \mathcal{C}_{\mathbb{R}^n}^{\leq}(x, c_i - x, \frac{\pi}{2})$. Therefore, $u(x)$ must be in the complement of the enclosing cone to the obstacle \mathcal{O}_i . Thus, one can conclude that $u(x) \in \mathcal{C}_{\mathbb{R}^n}^{\geq}(x, c_i - x, \frac{\pi}{2}) = \mathcal{T}_{\mathcal{F}}(x)$. Since $\forall x \in \mathcal{F}$, $u(x) \in \mathcal{T}_{\mathcal{F}}(x)$ and the solution of the closed-loop system (10)-(24) is unique, it follows that the free space \mathcal{F} is positively invariant and the closed-loop system (10)-(24) is safe.

Proof of Lemma 5

Let \mathcal{L}_i^e be the central half-line associated to obstacle \mathcal{O}_i , and let $y \in \mathcal{L}_i^e \setminus \mathcal{O}_i$. Since the control is tangent to the obstacle, for any $x \in \mathcal{AR}_i \setminus \mathring{\mathcal{H}}(y, c_i)$ the control, at a step p , can never point inside the hat $\mathring{\mathcal{H}}(y, c_k i)$, i.e., there is no position $q \in \mathcal{AR}_i \cap \mathring{\mathcal{H}}(y, c_i)$ such that $\angle(q - x, u_p(x)) = 0$, where $p = \iota_x^{-1}(i)$. Assume that $\mathcal{M}_i \neq \emptyset$ and consider an obstacle $k \in \mathcal{M}_i$ such that $k = \kappa_i^{-1}(1)$, $c_k \in \mathring{\mathcal{H}}(y, c_i)$, and $x_{k,i}^* = y$. Assume that $\mathring{\mathcal{H}}(x_{k,i}^*, c_i) \cap \mathcal{O}_l = \emptyset$ for all $l \in \mathbb{I} \setminus \{i, k\}$, which ensures that no other obstacle interferes and changes the direction of the control u_p towards the hat $\mathring{\mathcal{H}}(x_{k,i}^*, c_i)$. Consequently, there is no $x \in \mathcal{AR}_k \cap \mathcal{AR}_i$ such that $\angle(c_k - x, u_p) = \beta(c_k - x, u_p) = 0$ where $p = \iota_x^{-1}(i)$. Thus, obstacle k does not generate a set of undesired equilibria \mathcal{L}_k (see Fig. 24). Following the same reasoning, one can show that obstacle $j = \kappa_i^{-1}(2)$ will not generate a set of undesired equilibria by considering the obstacles \mathcal{O}_i and \mathcal{O}_k as single obstacle whose hat is the union $\mathring{\mathcal{H}}(x_{j,i}^*, c_i) \cup \mathring{\mathcal{H}}(x_{j,i}^*, c_k)$ and \mathcal{L}_i^e as its single central half-line since obstacle $k = \kappa_i^{-1}(1)$ is free of undesired equilibria. These considerations reduce to the first case where if $c_j \in \mathring{\mathcal{H}}(x_{j,i}^*, c_i) \cup \mathring{\mathcal{H}}(x_{j,i}^*, c_k)$ and $(\mathring{\mathcal{H}}(x_{j,i}^*, c_i) \cup \mathring{\mathcal{H}}(x_{j,i}^*, c_k)) \cap \mathcal{O}_l = \emptyset$ for all $l \in \mathbb{I} \setminus \{i, k\}$, obstacle j does not generate undesired equilibria. The same can be applied up to obstacle $\kappa_i^{-1}(p)$ by considering the union of the hat of obstacle i and obstacles \mathcal{M}_i^{p-1} , and the central half-line \mathcal{L}_i^e . Therefore, the obstacles of indices in the set \mathcal{M}_i^p are free of undesired equilibria if, for all $j \in \mathcal{M}_i^p$ with $p \in \{1, \dots, N_i\}$, 1) $c_j \in \cup_{l \in \mathcal{M}_i^{p-1}} \mathring{\mathcal{H}}(x_{j,i}^*, c_l)$ and 2) $\cup_{l \in \mathcal{M}_i^{p-1}} \mathring{\mathcal{H}}(x_{j,i}^*, c_l) \cap \mathcal{O}_z = \emptyset$ for all $z \in \mathbb{I} \setminus (\mathcal{M}_i^j \cup \{j\})$. If, in addition, $p = N_i$, or obstacle $\kappa_i^{-1}(p+1)$, with $p < N_i = \text{card}(\mathcal{M}_i)$, does not satisfy conditions 1) and 2), we say that $\bar{N}_i = p$ is the order of the set \mathcal{M}_i and the number of obstacles free of undesired equilibria with indices grouped in the set $\mathcal{M}_i^{\bar{N}_i}$, which concludes the proof.

Proof of Theorem 1

Item i) and item ii) follow directly from lemma 3 and lemma 4 respectively. Now let us prove item iii). Consider the set of undesired equilibria \mathcal{L}_i , $i \in \mathcal{Z}$. Define the tube surrounding \mathcal{L}_i inside the free space $\mathcal{TU}_i := \{x \in \mathcal{F} | d(x, \mathcal{L}_i) \leq e_i\}$ where e_i is small such that $\mathcal{TU}_i \subset \mathcal{AR}_i$, and $e_i < r_i$. Let $V(x) = \frac{1}{2}d^2(\mathcal{L}_i, x) = \frac{1}{2}(x - c_i)^\top \pi^\perp(\bar{v}_i)(x - c_i)$ where $\bar{v}_i = (\bar{x}_i - c_i)/\|\bar{x}_i - c_i\|$, $\bar{x}_i \in \mathcal{L}_i$, $V(x) = 0$ for all $x \in \mathcal{L}_i$, and $V(x) > 0$ for all $x \in \mathcal{TU}_i \setminus \mathcal{L}_i$. Let $U := \mathcal{TU}_i \cap \mathcal{P}_{\leq}(\bar{x}_i, \bar{v}_i) \setminus \mathcal{L}_i$ where $\bar{x}_i \in \mathcal{L}_i$ is such that $U \cap \mathcal{L}_k = \emptyset$ for all $k \in \mathcal{Z} \setminus \{i\}$, and $U \subset \mathcal{AR}_i^h$ with $\mathcal{AR}_i^h := \{q \in \mathcal{AR}_i | \iota_q^{-1}(i) = h(x)\}$. Note that $V(x) > 0$ for all $x \in U$. The time-derivative of $V(x)$ is given by $\dot{V}(x) = \frac{\partial V(x)}{\partial x}^\top \dot{x} = (x - c_i)^\top \pi^\perp(\bar{v}_i)u(x)$. Since $e_i < r_i$ and for all $x \in U$, $u(x)$ lies on the cone enclosing obstacle $\mathcal{O}_i \subset \mathcal{P}_{\leq}(\bar{x}_i, \bar{v}_i)$, $0 < \angle(\bar{v}_i, x - c_i) < \pi/2$ and $\pi/2 < \angle(\bar{v}_i, u(x)) < \pi$. Therefore, $\dot{V}(x) > 0$ for all $x \in U$. As U is a compact set, $V(x)$ is increasing on U , and $V(x) = 0$ on \mathcal{L}_i (the axis of the tube), $x(t)$ must leave the set U . The set U is bounded on top by obstacle i , its lateral boundary is the surface of the tube, and is bounded from the bottom by the hyperplane $\mathcal{P}_{=}(\bar{x}_i, \bar{v}_i)$. Due to the safety of the system, as per Lemma 3, $x(t)$ can not leave U from the upper boundary (the boundary of obstacle i), and since $\pi/2 < \angle(\bar{v}_i, u(x)) < \pi$, $x(t)$ can only leave U from the surface of the tube. Now, let us prove item iv). Since $x_d \in \mathcal{VI}$, there exists $r_d > 0$ such that $\mathcal{B}(x_d, r_d) \subset \mathcal{VL}$. As the closed-loop system (10)-(24) reduces to $\dot{x} = -\gamma(x - x_d)$ on the visible set \mathcal{VI} , the equilibrium $x = x_d$ is locally exponentially stable. Finally, let us prove item v). Since the control input (24) is a composition of the projection from Lemma 1, which generates the shortest path for a considered obstacle, according to Lemma 6, the trajectory $x(t)$ of the closed-loop system (10)-(24) is generated by a quasi-optimal obstacle avoidance maneuver, for $\varepsilon = 0$, as per Definition 1.

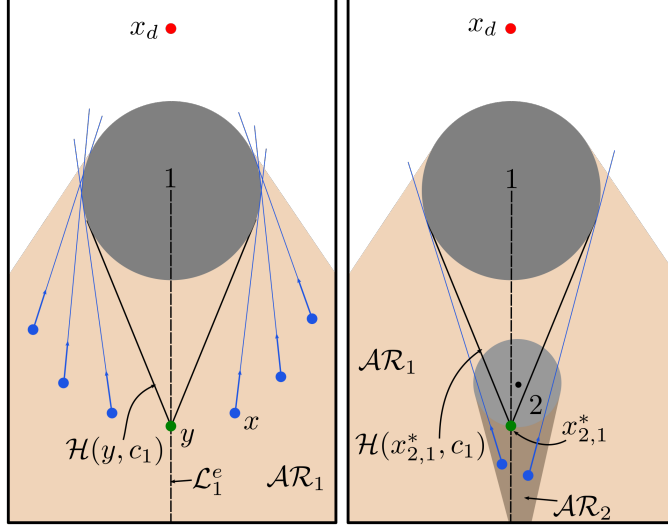


Figure 24: The left figure shows that for all position $x \in \mathcal{AR}_1 \setminus \mathcal{H}(y, c_1)$, the control cannot point inside $\mathcal{H}(y, c_1)$. In the right figure, obstacle 2 is placed such that $c_2 \in \mathcal{H}(y, c_1)$, the intermediary control u_1 cannot point inside $\mathcal{H}(y, c_1)$ and $y = x_{2,1}^*$. Then, the intermediary control u_1 cannot point into the center c_2 at any position $x \in \mathcal{AR}_2$ which implies that \mathcal{L}_2 is an empty set.

Proof of Lemma 6

Let $i \in \mathbb{L}$. Since \mathbf{Cell}_i is bounded by line segments of undesired equilibria ($\cup_{k \in \mathcal{Z}} \mathcal{L}_k$) and the free space boundary, $u(x)$ points inside the cell when $x \in \partial \mathbf{Cell}_i \cap \partial \mathcal{F}$, as per Lemma 3, and $u(x) = 0$ when $x \in \partial \mathbf{Cell}_i \cap (\cup_{k \in \mathcal{Z}} \mathcal{L}_k)$. Consequently, \mathbf{Cell}_i is forward invariant for the closed-loop system (10)-(24).

Proof of Lemma 7

Since the nests are invariant, as per Lemma 6, and all the undesired equilibria are contained inside the nests, it remains to show that if we start outside nests, we'll never get back in. We begin with the special nest ($\mathbf{Nest}_0 = \cup_{i \in \mathcal{Z}} \mathcal{L}_i \setminus \cup_{j \in \mathbb{L}} \mathbf{Cell}_j$) formed by segments of undesired equilibria and show their repellency. These segments can be defined as $\mathcal{CL}_i := \{q \in \mathcal{L}_i \mid q \notin \cup_{k \in \mathbb{L}} \mathbf{Cell}_k\} \subset \mathbf{Nest}_0$ for $i \in \mathcal{Z}$.

Consider obstacle $i \in \mathcal{Z}$ and segment \mathcal{CL}_i in the following three possible cases illustrated in (Fig. 25):

Case 1: Consider the region $\mathcal{AR}_i^h := \{q \in \mathcal{AR}_i \mid \iota_q^{-1}(i) = h(q)\}$ where obstacle i is the last on the list of projections. Define the tube $\mathcal{TU}_i := \{x \in \mathcal{F} \mid d(x, \mathcal{CL}_i) \leq e_i\}$ where e_i is small enough to have $\mathcal{TU}_i \cap \mathcal{L}_j = \emptyset$ for all $j \in \mathcal{Z} \setminus \{i\}$ and $\mathcal{TU}_i \subset \mathcal{AR}_i$. Let $V(x) = 1 - \frac{(\bar{x}_i - c_i)^\top (x - c_i)}{\|\bar{x}_i - c_i\| \|x - c_i\|}$ where $\bar{x}_i \in \mathcal{CL}_i \cap \mathcal{AR}_i^h$. Note that $V(\bar{x}_i) = 0$, and $V(x) > 0$ for all $x \in \mathcal{TU}_i \setminus \mathcal{CL}_i$. Define the set $U := (\mathcal{TU}_i \cap \mathcal{AR}_i^h) \setminus \mathcal{CL}_i$. The time-derivative of $V(x)$ is given by

$$\begin{aligned}\dot{V}(x) &= \frac{\partial V(x)}{\partial x}^\top \dot{x}, \\ &= -\frac{(\bar{x}_i - c_i)^\top}{\|\bar{x}_i - c_i\|} J_x \left(\frac{(x - c_i)}{\|x - c_i\|} \right) u(x), \\ &= -K \bar{V}_{ci}^\top \pi^\perp(V_{ci}) \bar{\xi}_i,\end{aligned}$$

where $K = \frac{\|u(x)\|}{\|x - c_i\|} > 0$, $V_{ci} = \frac{(c_i - x)}{\|c_i - x\|}$, $\bar{V}_{ci} = \frac{(\bar{x}_i - c_i)}{\|\bar{x}_i - c_i\|}$ and $\bar{\xi}_i = \frac{\sin(\theta_i) u_{h(x)-1}}{\sin(\beta_i) \|u_{h(x)-1}\|} - \frac{\sin(\theta_i - \beta_i)}{\sin(\beta_i)} V_{ci}$.

The segment \mathcal{CL}_i divides the set \mathcal{AR}_i^h into two symmetric regions, a left-side $\mathcal{P}_<(c_i, R_1 \bar{V}_{ci}) \cap \mathcal{AR}_i^h$, and a right-side $\mathcal{P}_>(c_i, R_1 \bar{V}_{ci}) \cap \mathcal{AR}_i^h$. On the right side, the control is on the right tangent to obstacle i , while on the left, the control is on the right tangent to obstacle i . Therefore, the control can not point inside the region enclosed by the vectors \bar{V}_{ci} , V_{ci} (i.e., $\forall x \in \mathcal{AR}_i^h \setminus \mathcal{CL}_i$, $u(x) \notin \{v \in \mathbb{R}^n \mid v = a\bar{V}_{ci} + bV_{ci}, a > 0, b > 0\}$). Thus, for all $x \in U$, $\bar{V}_{ci}^\top \bar{\xi}_i = \cos(\sigma_i + \theta_i)$

where $0 < \sigma_i = \angle(\bar{V}_{ci}, V_{ci}) < \pi$ and $0 < \theta_i = \angle(V_{ci}, \bar{\xi}_i) \leq \frac{\pi}{2}$. Then,

$$\begin{aligned}\dot{V}(x) &= -K (\cos(\sigma_i + \theta_i) - \cos(\sigma_i) \cos(\theta_i)), \\ &= K \sin(\sigma_i) \sin(\theta_i).\end{aligned}$$

Therefore, $\dot{V}(\bar{x}_i) = 0$ and $\dot{V}(x) > 0$ for all $x \in U$.

Case 2: Consider the region \mathcal{AR}_k^h where $k \in \mathcal{M}_i^{\bar{N}_i}$. Define the tube $\mathcal{TU}_i := \{x \in \mathcal{F} | d(x, \mathcal{CL}_i) \leq e_i\}$ where e_i is small such that $\mathcal{TU}_i \cap \mathcal{L}_j = \emptyset$ for all $j \in \mathcal{Z} \setminus \{i\}$, and $\mathcal{TU}_i \subset \mathcal{AR}_k$. Let $V(x) = 1 - \frac{(\bar{x}_i - x_{k,i}^*)^\top}{\|\bar{x}_i - x_{k,i}^*\|} \frac{(x - x_{k,i}^*)}{\|x - x_{k,i}^*\|}$ where $\bar{x}_i \in \mathcal{CL}_i \cap \mathcal{AR}_k^h$ and $x_{k,i}^* = \arg \max_{q \in \mathcal{L}_i^e \cap \partial \mathcal{O}_k} \|c_i - q\|$. Note that $V(\bar{x}_i) = 0$, and $V(x) > 0$ for all $x \in (\mathcal{TU}_i \cap \mathcal{AR}_k^h) \setminus \mathcal{CL}_i$.

Define the set $U := (\mathcal{TU}_i \cap \mathcal{AR}_k^h) \setminus \mathcal{CL}_i$. The time-derivative of $V(x)$ is given by

$$\begin{aligned}\dot{V}(x) &= \frac{\partial V(x)}{\partial x}^\top \dot{x}, \\ &= -\frac{(\bar{x}_i - x_{k,i}^*)^\top}{\|\bar{x}_i - x_{k,i}^*\|} J_x \left(\frac{(x - x_{k,i}^*)}{\|x - x_{k,i}^*\|} \right) u(x), \\ &= -K \bar{V}_{k,i}^\top \pi^\perp(V_{k,i}) \bar{\xi}_k,\end{aligned}$$

where $K = \frac{\|u(x)\|}{\|x - x_{k,i}^*\|} > 0$, $V_{k,i} = \frac{(x_{k,i}^* - x)}{\|x_{k,i}^* - x\|}$, $\bar{V}_{k,i} = \frac{(\bar{x}_i - x_{k,i}^*)}{\|\bar{x}_i - x_{k,i}^*\|}$ and $\bar{\xi}_k = \frac{\sin(\theta_k) u_{h(x)-1}}{\sin(\beta_k) \|u_{h(x)-1}\|} - \frac{\sin(\theta_k - \beta_k)}{\sin(\beta_k)} V_{ck}$. Similar to the previous case, segment \mathcal{CL}_i divides set \mathcal{AR}_k^h into two regions, a left-side $\mathcal{P}_<(c_i, R_1 \bar{V}_{k,i}) \cap \mathcal{AR}_k^h$ and a right-side $\mathcal{P}_>(c_i, R_1 \bar{V}_{k,i}) \cap \mathcal{AR}_k^h$. On the right side, the control is on the right tangent to obstacle k , while on the left, the control is on the left tangent to obstacle k . Therefore, by considering $V_{k,i}$ instead of V_{ck} where $V_{k,i} = a \bar{V}_{k,i} + b V_{ck}$, $a > 0$, $b > 0$, $0 < \sigma_{k,i} = \angle(\bar{V}_{k,i}, V_{k,i}) < \pi$, and $\theta_k < \theta_k^* = \angle(\bar{V}_{k,i}, \bar{\xi}_k) < \pi$, we can write $\bar{V}_{k,i}^\top \bar{\xi}_k = \cos(\sigma_{k,i} + \theta_k^*)$ for all $x \in U$. Then,

$$\begin{aligned}\dot{V}(x) &= -K (\cos(\sigma_{k,i} + \theta_k^*) - \cos(\sigma_{k,i}) \cos(\theta_k^*)), \\ &= K \sin(\sigma_{k,i}) \sin(\theta_k^*),\end{aligned}$$

Therefore, $\dot{V}(\bar{x}_i) = 0$ and $\dot{V}(x) > 0$ for all $x \in U$.

Case 3: Consider the region \mathcal{AR}_k^h where $\mathcal{L}_i^e \cap \mathcal{O}_k = \emptyset$ and $\mathcal{CL}_i \cap \mathcal{AR}_k^h \neq \emptyset$. Let $\bar{\Omega}_i = R_b(c_i - \bar{x}_i)$ where $\bar{x}_i \in \mathcal{CL}_i \cap \mathcal{AR}_k^h$, $R_b = \begin{pmatrix} 0 & b \\ -b & 0 \end{pmatrix}$, and $b \in \{-1, 1\}$ is chosen such that $\bar{\Omega}_i^\top (c_k - \bar{x}_i) > 0$. Since $c_k \in \mathcal{P}_>(\bar{x}_i, \bar{\Omega}_i)$ and $\mathcal{L}_i^e \cap \mathcal{O}_k = \emptyset$, $\mathcal{O}_k \subset \mathcal{P}_>(\bar{x}_i, \bar{\Omega}_i)$. Define the tube $\mathcal{TU}_i := \{x \in \mathcal{F} | d(x, \mathcal{CL}_i) \leq e_i\}$ where e_i is small such that $\mathcal{TU}_i \cap \mathcal{P}_>(\bar{x}_i, \bar{\Omega}_i) \cap \mathcal{L}_j = \emptyset$ for all $j \in \mathcal{Z} \setminus \{i\}$, and $\bar{\Omega}_i^\top u(x) > 0$ for all $x \in \mathcal{TU}_i \cap \mathcal{P}_>(\bar{x}_i, \bar{\Omega}_i)$. Let $V(x) = \bar{\Omega}_i^\top (x - \bar{x}_i)$ where $V(\bar{x}_i) = 0$ and $V(x) > 0$ for all $x \in \mathcal{P}_>(\bar{x}_i, \bar{\Omega}_i)$. Define the set $U := \mathcal{TU}_i \cap \mathcal{P}_>(\bar{x}_i, \bar{\Omega}_i) \cap \mathcal{AR}_k^h$.

$$\dot{V}(x) = \frac{\partial V(x)}{\partial x}^\top \dot{x} = \bar{\Omega}_i^\top u(x),$$

where $\dot{V}(x) > 0$ for all $x \in U$ and $\dot{V}(x) = 0$ for $x \in \mathcal{CL}_i$.

In the three treated cases, U is compact, $V(x) = 0$ on the undesired equilibria \mathcal{CL}_i , and V is increasing on U . Therefore, $x(t)$ must leave U .

Now, we will show that if we start outside a given nest Nest_k , $k > 0$, we will never get inside any nest. Consider the nest Nest_k , obstacle $j \in \mathbb{L}$, and the set of undesired equilibria \mathcal{L}_i such that $k > 0$, $i \in \mathcal{R}_j$, and $\partial \text{Nest}_k \cap \mathcal{L}_i \cap \mathcal{AR}_j^h \neq \emptyset$ (i.e., segment (or segments) of \mathcal{L}_i forms a portion of the boundary of the nest Nest_k when the last projection involves obstacle j). Define the tube $\mathcal{TU}_i := \{x \in \mathcal{F} | d(x, \mathcal{L}_i \cap \mathcal{AR}_j^h) \leq e_i\}$ where e_i is small such that $(\mathcal{TU}_i \setminus \text{Nest}_k) \cap \mathcal{L}_p = \emptyset$ for all $p \in \mathcal{Z} \setminus \{i\}$, and $\mathcal{TU}_i \subset \mathcal{AR}_j$. This case amounts to case 2) with $U := (\mathcal{TU}_i \setminus \text{Nest}_k) \cap \mathcal{AR}_j^h$. Since the nests are invariants, $\cup_{i \in \mathcal{Z}} \mathcal{L}_i \subset \cup_k \text{Nest}_k$, and for all $x(0) \notin \cup_k \text{Nest}_k$, $\lim_{t \rightarrow +\infty} x(t) \notin \text{Nest}_k$, the set of nests $\cup_k \text{Nest}_k$, is the attraction region of the undesired equilibria.

Proof of Theorem 2

Item i) follow directly from Lemma 7. According to item v) of Theorem 1, all trajectories converging to x_d are generated by a quasi-optimal obstacle avoidance maneuver and item i) states that x_d is attractive from all $x(0) \in \mathcal{F} \setminus \cup_k \text{Nest}_k$, which proves item ii). Since Assumption 3 imposes that $\mathbb{L} = \emptyset$, no cell will be created, which implies that only the special nest exists. Therefore, $\cup_k \text{Nest}_k = \text{Nest}_0 = \cup_{i \in \mathcal{Z}} \mathcal{L}_i$ is the region of attraction of the undesired equilibria $\cup_{i \in \mathcal{Z}} \mathcal{L}_i$, as per Lemma 7, and has Lebesgue measure zero, which shows the almost global asymptotic stability of x_d .

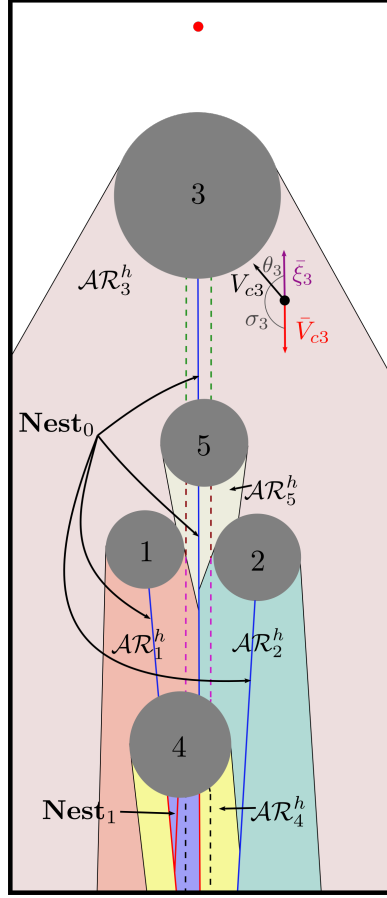


Figure 25: Illustration of the nests (attraction region of the undesired equilibria.)

Proof of Lemma 8

Let us look for the equilibria of the closed-loop system (10)-(35) by setting $u(x) = 0$. Then, from the first equation of (35), the equilibrium point is x_d . From the second equation of (35), one gets $u_d(x) = \|u_d(x)\| \frac{\sin(\tilde{\theta} - \tilde{\beta})}{\sin(\tilde{\theta})} \frac{\tilde{c} - x}{\|\tilde{c} - x\|}$ which is true if and only if $\tilde{\beta} = 0$ (i.e., $\angle(u_d, (\tilde{c} - x)) = 0$). As $\widetilde{\mathcal{BL}}$ is the union of the disjoints practical shadow regions, there exists a unique $i \in \mathbb{I}$ such that if $x \in \widetilde{\mathcal{BL}}$, $x \in \tilde{\mathcal{D}}(x_d, c_i, R)$, and since \tilde{c} is the projection of x onto obstacle i , $\frac{\tilde{c} - x}{\|\tilde{c} - x\|} = \frac{c_i - x}{\|c_i - x\|}$. Therefore, $u(x) = 0$ for all $x \in \tilde{\mathcal{L}}_d(x_d, c_i, R) := \mathcal{L}_d(x_d, c_i) \cap \tilde{\mathcal{D}}(x_d, c_i, R)$ where $\mathcal{L}_d(x_d, c_i)$ is defined in Lemma 2. First-generation obstacles have the following property, $\forall x \in \mathcal{D}(x_d, c_i)$, $i = \iota_x(1)$, which implies that the undesired equilibria of a first-generation obstacle are characterized by the angle $\beta_i(u_d(x), x) = 0$ for all $x \in \mathcal{D}(x_d, c_i)$. Since, in the sensor-based case, $h(x) = \text{card}(\mathcal{I}(x)) = 1$ for all $x \in \widetilde{\mathcal{BL}}$, all the obstacles are first-generation obstacles under (35), and since $\beta_i(u_d(x), x) = \angle(u_d(x), c_i - x)$, $\mathcal{L}_i = \mathcal{L}_d(x_d, c_i)$. Finally, one can conclude that the set of undesired equilibria for the closed-loop system (10)-(35) is $\zeta = \{x_d\} \cup \left(\cup_{i \in \mathbb{I}} \tilde{\mathcal{L}}_d(x_d, c_i, R) \right)$ where the sets of undesired equilibria $\tilde{\mathcal{L}}_d(x_d, c_i, R)$ are the sets \mathcal{L}_i limited to the practical shadow regions.

Proof of Theorem 3

Since the sensor-based case is a special case of the map-based scenario when all the obstacles are first-generation obstacles, item i) follows from item i) of Theorem 1. Item ii) follows directly from Lemma 8. Now, let us prove item iii). Consider obstacle $i \in \mathbb{I}$ and the set of equilibrium points $\tilde{\mathcal{L}}_d(x_d, c_i, R)$. Define the tube $\mathcal{TU}_i := \{x \in \tilde{\mathcal{D}}(x_d, c_i, R) | d(x, \tilde{\mathcal{L}}_d(x_d, c_i, R)) \leq e_i\}$ surrounding $\tilde{\mathcal{L}}_d(x_d, c_i, R)$ inside the practical shadow region where e_i is small such that $\tilde{c} = \arg \min_{y \in \mathcal{O}_i} \|x - y\|$. Let $V(x) = 1 - \frac{(\tilde{x}_i - c_i)^\top (x - \tilde{c})}{\|\tilde{x}_i - c_i\| \|x - \tilde{c}\|}$ where $\tilde{x}_i \in \tilde{\mathcal{L}}_d(x_d, c_i, R)$. Note that $V(\tilde{x}_i) = 0$ and

$V(x) > 0$ for all $x \in \mathcal{TU}_i \setminus \tilde{\mathcal{L}}_d(x_d, c_i, R)$. Define the set $U := \{x \in \mathcal{TU}_i | V(x) > 0\}$. The time-derivative of $V(x)$ on \mathcal{TU}_i is given by

$$\begin{aligned}\dot{V}(x) &= \frac{\partial V(x)}{\partial x}^\top \dot{x}, \\ &= -\frac{(\tilde{x}_i - c_i)^\top}{\|\tilde{x}_i - c_i\|} J_x \left(\frac{(x - \tilde{c})}{\|x - \tilde{c}\|} \right) u(x), \\ &= \frac{-1}{\|\tilde{x}_i - c_i\| \|x - \tilde{c}\|} (\tilde{x}_i - c_i)^\top \pi^\perp \left(\frac{(x - \tilde{c})}{\|x - \tilde{c}\|} \right) u(x), \\ &= \frac{-\gamma}{\|\tilde{x}_i - c_i\| \|x - \tilde{c}\|} (\tilde{x}_i - c_i)^\top \pi^\perp \left(\frac{(x - \tilde{c})}{\|x - \tilde{c}\|} \right) (x_d - x), \\ &= -K(\tilde{x}_i - c_i)^\top \pi^\perp (V_{ci})(x_d - x),\end{aligned}$$

where $K = \frac{\gamma}{\|\tilde{x}_i - c_i\| \|x - \tilde{c}\|}$, and as \tilde{c} is the projection of x onto obstacle i for all $x \in \mathcal{TU}_i$, $V_{ci} = \frac{(c_i - x)}{\|c_i - x\|} = \frac{(\tilde{c} - x)}{\|\tilde{c} - x\|}$. Since $\tilde{x}_i = c_i + \delta \frac{c_i - x_d}{\|c_i - x_d\|}$ with $\delta \geq r_i$, one gets

$$\begin{aligned}\dot{V}(x) &= -\frac{\delta K}{\|c_i - x_d\|} (c_i - x_d)^\top \pi^\perp (V_{ci})(x_d - x), \\ &= -\frac{\delta K}{\|c_i - x_d\|} ((c_i - x) + (x - x_d))^\top \pi^\perp (V_{ci})(x_d - x), \\ &= \frac{\delta K}{\|c_i - x_d\|} (x_d - x)^\top \pi^\perp (V_{ci})(x_d - x).\end{aligned}$$

where we used the fact that $(c_i - x)^\top \pi^\perp (V_{ci})(x_d - x) = 0$. It is clear that $\dot{V}(x) > 0$ for all $x \in U$, and $\dot{V}(x) = 0$ for all $x \in \tilde{\mathcal{L}}_d(x_d, c_i, R)$ over the set \mathcal{TU}_i . Since U is a compact set, $V(x)$ is increasing on U , and $V(x) = 0$ on $\tilde{\mathcal{L}}_d(x_d, c_i, R)$ (the tube axis), $x(t)$ must leave the set U . Note that the set U is bounded by the free space boundary and the lateral surface of tube \mathcal{TU}_i . Due to the safety of the system, as per item i), $x(t)$ can not leave U from the free space boundary and can only leave it from the surface of the tube for all $x(0) \in U$. Therefore, the set of equilibria $\tilde{\mathcal{L}}_d(x_d, c_i, R)$ is unstable. Lastly, we prove item iv). Consider the equilibrium point x_d and the positive definite function $V_1(x) = \frac{1}{2} \|x - x_d\|^2$ whose time-derivative is given by

$$\begin{aligned}\dot{V}_1(x) &= \frac{\partial V_1(x)}{\partial x}^\top \dot{x}, \\ &= (x - x_d)^\top u(x), \\ &= \begin{cases} -\gamma \|x - x_d\|^2, & x \in \widetilde{\mathcal{VI}} \\ -\gamma \|x - x_d\|^2 + \gamma \|x - x_d\| \frac{\sin(\tilde{\theta} - \tilde{\beta})}{\sin(\tilde{\theta})} \frac{(x_d - x)^\top (\tilde{c} - x)}{\|\tilde{c} - x\|}, & x \in \widetilde{\mathcal{BL}} \end{cases} \\ &= \begin{cases} -\gamma \|x - x_d\|^2, & x \in \widetilde{\mathcal{VI}} \\ -\gamma \|x - x_d\|^2 + \gamma \|x - x_d\|^2 \frac{\sin(\tilde{\theta} - \tilde{\beta})}{\sin(\tilde{\theta})} \cos(\tilde{\beta}), & x \in \widetilde{\mathcal{BL}} \end{cases} \\ &= \begin{cases} -\gamma \|x - x_d\|^2, & x \in \widetilde{\mathcal{VI}} \\ -\gamma \|x - x_d\|^2 \frac{\sin(\tilde{\beta})}{\sin(\tilde{\theta})} \cos(\tilde{\theta} - \tilde{\beta}), & x \in \widetilde{\mathcal{BL}} \end{cases}\end{aligned}$$

where we used the fact that $\sin(\tilde{\theta}) - \sin(\tilde{\theta} - \tilde{\beta}) \cos(\tilde{\beta}) = \sin(\tilde{\beta}) \cos(\tilde{\theta} - \tilde{\beta})$, $0 < \tilde{\theta} \leq \frac{\pi}{2}$ and $0 \leq \tilde{\beta} \leq \tilde{\theta}$. Therefore, $\dot{V}_1(x) = 0$ only for $x \in \zeta$ and $\dot{V}_1(x) < 0$ for all $x \in \mathcal{F} \setminus \zeta$. Since the practical shadow regions are disjoint by construction, and the undesired equilibria $\tilde{\mathcal{L}}_d(x_d, c_i, R)$ are limited to the shadow regions as per Lemma 8, $\mathbb{L} = \emptyset$ and $\mathbf{Cell}_i = \emptyset$ for all $i \in \mathbb{I}$. Thus, for all $i \in \mathbb{I}$, the attraction region of the set of undesired equilibria $\tilde{\mathcal{L}}_d(x_d, c_i, R)$ reduces to the line segment $\mathcal{L}_d(x_d, c_i) \cap \mathcal{D}^t(x_d, c_i)$. Since the attraction region of the undesired equilibria is a set of measure zero, the equilibrium point x_d is almost globally asymptotically stable in \mathcal{F} .

Proof of Lemma 9

Following the same procedure as in 9, $u(x) = 0$ if and only if $x = x_d$ or $x \in \tilde{\mathcal{L}}_d(x_d, x_i, R)$, where for all $x \in \tilde{\mathcal{L}}_d(x_d, x_i, R)$, $\tilde{c} = x_i$ and $\frac{(\tilde{c}-x)^\top (x_d-x)^\top}{\|\tilde{c}-x\| \|x_d-x\|} = 1$. Therefore, one can conclude that the set of equilibria is $\tilde{\zeta} = \{x_d\} \cup \left(\cup_{i \in \mathbb{I}} \tilde{\mathcal{L}}_d(x_d, x_i, R) \right)$.

Proof of Theorem 4

Since the considered convex obstacles have smooth boundaries, the tangent cone on the boundaries of the obstacles are half-planes, which is similar to the spherical obstacles case. Therefore, item i) follows from item i) of Theorem 3. Item ii) follows directly from Lemma 9. Now, let us prove item iii). Consider obstacle $i \in \mathbb{I}$ and the equilibrium point $\bar{x}_i \in \tilde{\mathcal{L}}_d(x_d, x_i, R)$. Define the tube $\mathcal{TU}_i := \{x \in \tilde{\mathcal{D}}(x_d, i, R) | d(x, \tilde{\mathcal{L}}_d(x_d, x_i, R)) \leq e_i\}$ surrounding $\tilde{\mathcal{L}}_d(x_d, x_i, R)$ inside the practical shadow region where e_i is small such that $\tilde{c} = \arg \min_{y \in \tilde{\mathcal{O}}_i} \|x - y\|$. Let $V(x) = 1 - \frac{(\bar{x}_i - c_i)^\top (x - \tilde{c})}{\|\bar{x}_i - c_i\| \|x - \tilde{c}\|}$

where $\tilde{x}_i \in \tilde{\mathcal{L}}_d(x_d, x_i, R)$. Note that $V(\tilde{x}_i) = 0$ and $V(x) > 0$ for all $x \in \mathcal{TU}_i \setminus \tilde{\mathcal{L}}_d(x_d, x_i, R)$. Define the set $U := \{x \in \mathcal{TU}_i | V(x) > 0\}$. The time-derivative of $V(x)$ on \mathcal{TU}_i is given by

$$\begin{aligned} \dot{V}(x) &= \frac{\partial V(x)}{\partial x}^\top \dot{x}, \\ &= -\frac{(\bar{x}_i - x_d)^\top}{\|\bar{x}_i - x_d\|} J_x \left(\frac{(x - x_d)}{\|x - x_d\|} \right) u(x), \\ &= \frac{-1}{\|x - x_d\|} \frac{(x - x_d)^\top}{\|\bar{x}_i - x_d\|} \pi^\perp \left(\frac{(x - x_d)}{\|x - x_d\|} \right) u(x), \\ &= \frac{\gamma \sin(\tilde{\theta} - \tilde{\beta})}{\sin(\tilde{\theta})} \frac{(\bar{x}_i - x_d)^\top}{\|\bar{x}_i - x_d\|} \pi^\perp \left(\frac{(x - x_d)}{\|x - x_d\|} \right) \frac{(\tilde{c} - x)}{\|\tilde{c} - x\|}, \\ &= K(-\cos(\tilde{\phi}) + \cos(\phi_d) \cos(\tilde{\beta})), \end{aligned}$$

where $K = \frac{\gamma \sin(\tilde{\theta} - \tilde{\beta})}{\sin(\tilde{\theta})}$, $\tilde{\phi} = \angle(\bar{x}_i - x_d, x - \tilde{c})$, $0 < \phi_d = \angle(\bar{x}_i - x_d, x - x_d) \leq \phi_d^{max}$, and $\phi_d^{max} = \arcsin(e_i / \|x - x_d\|) \in (0, \pi/2]$. Since obstacle i satisfies the curvature condition, as per Assumption 4, and \tilde{c} is the projection of x onto obstacle i , $0 < \tilde{\phi} = \phi_d + \tilde{\beta} < \pi$, where $0 \leq \tilde{\beta} = \angle(\tilde{c} - x, x_d - x) \leq \frac{\pi}{2}$. Thus,

$$\dot{V}(x) = K \sin(\phi_d) \sin(\tilde{\beta}).$$

It is clear that, over the set \mathcal{TU}_i , $\dot{V}(x) = 0$ for $x \in \tilde{\mathcal{L}}_d(x_d, x_i, R)$ (i.e., $\tilde{\beta} = 0$), and $\dot{V}(x) > 0$ for all $x \in U$. Since U is a compact set, $V(x)$ is increasing on U , and $V(x) = 0$ on $\tilde{\mathcal{L}}_d(x_d, x_i, R)$ (the tube axis), $x(t)$ must leave the set U . Note that the set U is bounded by the free space boundary and the lateral surface of tube \mathcal{TU}_i . Due to the safety of the system, as per item i), $x(t)$ can not leave U from the free space boundary and can only leave it from the surface of the tube for all $x(0) \in U$. Therefore, the set of equilibria $\tilde{\mathcal{L}}_d(x_d, x_i, R)$ is unstable.

Finally, proof of item iv) is similar to that of item iv) in 9.

References

- Ishak Cheniouni, Abdelhamid Tayebi, and Soulaimane Berkane. Safe and quasi-optimal autonomous navigation in sphere worlds. In *2023 American Control Conference (ACC)*, pages 2678–2683, 2023. doi:10.23919/ACC55779.2023.10156634.
- Edsger W. Dijkstra. A note on two problems in connexion with graphs. *Numerische Mathematik*, 1:269–271, 1959.
- Peter E. Hart, Nils J. Nilsson, and Bertram Raphael. A formal basis for the heuristic determination of minimum cost paths. *IEEE Transactions on Systems Science and Cybernetics*, 4(2):100–107, 1968. doi:10.1109/TSSC.1968.300136.
- V. Lumelsky and A. Stepanov. Dynamic path planning for a mobile automaton with limited information on the environment. *IEEE Transactions on Automatic Control*, 31(11):1058–1063, 1986. doi:10.1109/TAC.1986.1104175.
- V.J. Lumelsky and T. Skewis. Incorporating range sensing in the robot navigation function. *IEEE Transactions on Systems, Man, and Cybernetics*, 20(5):1058–1069, 1990. doi:10.1109/21.59969.

- Oussama Khatib. Real time obstacle avoidance for manipulators and mobile robots. *The International Journal of Robotics Research*, 5(1):90–99, 1986.
- Daniel E. Koditschek and Elon D. Rimon. Robot Navigation Functions on Manifolds with Boundary. *ADVANCES IN APPLIED MATHEMATICS*, 11:412–442, 1990.
- Elon D. Rimon and Daniel E. Koditschek. The construction of analytic diffeomorphisms for exact robot navigation on star worlds. *Transactions of the American Mathematical Society*, 327(1):71–116, 1991.
- Elon D. Rimon and Daniel E. Koditschek. Exact Robot Navigation Using Artificial Potential Functions. *IEEE Transactions on Robotics and Automation*, 8(5):501–518, 1992.
- S. G. Loizou. The navigation transformation: Point worlds, time abstractions and towards tuning-free navigation. In *2011 19th Mediterranean Conference on Control Automation (MED)*, pages 303–308, 2011. doi:10.1109/MED.2011.5983166.
- Nicolas Constantinou and Savvas G. Loizou. Robot navigation on star worlds using a single-step navigation transformation. In *2020 59th IEEE Conference on Decision and Control (CDC)*, pages 1537–1542, 2020. doi:10.1109/CDC42340.2020.9303745.
- Santiago Paternain, Daniel E. Koditschek, and Alejandro Ribeiro. Navigation functions for convex potentials in a space with convex obstacles. *IEEE Transactions on Automatic Control*, 63(9):2944–2959, 2018. doi:10.1109/TAC.2017.2775046.
- S. G. Loizou and Elon D. Rimon. Correct-by-construction navigation functions with application to sensor based robot navigation, 2021.
- Omur Arslan and Daniel E Koditschek. Sensor-based reactive navigation in unknown convex sphere worlds. *The International Journal of Robotics Research*, 38(2-3):196–223, 2019. doi:10.1177/0278364918796267.
- V. G. Vasilopoulos and D. E. Koditschek. Reactive Navigation in Partially Known Non-Convex Environments. In *13th International Workshop on the Algorithmic Foundations of Robotics (WAFR)*, 2018.
- Vasileios G. Vasilopoulos, Georgios Pavlakos, Karl Schmeckpeper, Kostas Daniilidis, and Daniel E. Koditschek. Reactive navigation in partially familiar planar environments using semantic perceptual feedback. *ArXiv*, abs/2002.08946, 2020.
- Mitio Nagumo. Über die lage der integralkurven gewöhnlicher differentialgleichungen. *Proceedings of the Physico-Mathematical Society of Japan. 3rd Series*, 24:551–559, 1942. doi:10.11429/ppmsj1919.24.0_551.
- Soulaimane Berkane. Navigation in unknown environments using safety velocity cones. In *2021 American Control Conference (ACC)*, pages 2336–2341, 2021. doi:10.23919/ACC50511.2021.9482911.
- Aaron D. Ames, Jessy W. Grizzle, and Paulo Tabuada. Control barrier function based quadratic programs with application to adaptive cruise control. In *53rd IEEE Conference on Decision and Control*, pages 6271–6278, 2014. doi:10.1109/CDC.2014.7040372.
- Aaron D. Ames, Xiangru Xu, Jessy W. Grizzle, and Paulo Tabuada. Control barrier function based quadratic programs for safety critical systems. *IEEE Transactions on Automatic Control*, 62(8):3861–3876, 2017. doi:10.1109/TAC.2016.2638961.
- R.G. Sanfelice, M.J. Messina, S. Emre Tuna, and A.R. Teel. Robust hybrid controllers for continuous-time systems with applications to obstacle avoidance and regulation to disconnected set of points. In *2006 American Control Conference*, pages 6 pp.–, 2006. doi:10.1109/ACC.2006.1657236.
- Soulaimane Berkane, Andrea Bisoffi, and Dimos V. Dimarogonas. Obstacle avoidance via hybrid feedback. *IEEE Transactions on Automatic Control*, 67(1):512–519, 2022. doi:10.1109/TAC.2021.3086329.
- Mayur Sawant, Soulaimane Berkane, Ilia Polushin, and Abdelhamid Tayebi. Hybrid feedback for autonomous navigation in planar environments with convex obstacles. *IEEE Transactions on Automatic Control*, pages 1–16, 2023a. doi:10.1109/TAC.2023.3277884.
- S. Berkane, A. Bisoffi, and D. V. Dimarogonas. A hybrid controller for obstacle avoidance in an n -dimensional euclidean space. In *2019 18th European Control Conference (ECC)*, pages 764–769, 2019. doi:10.23919/ECC.2019.8795713.
- Franco Blanchini and Stefano Miani. *Set-Theoretic Methods in Control*. Birkhäuser Basel, 1st edition, 2007. ISBN 0817632557.
- Mayur Sawant, Abdelhamid Tayebi, and Ilia Polushin. Hybrid feedback control design for non-convex obstacle avoidance. *arXiv:2304.10598*, 2023b.
- Jorge Cortes. Discontinuous dynamical systems. *IEEE Control Systems Magazine*, 28(3):36–73, 2008. doi:10.1109/MCS.2008.919306.